Therefore, in the female germline, as represented by the phES cells, a subset of imprinted loci retain their identity in the absence of methylation, suggesting that additional epigenetic mechanisms mark these regions for maternal methylation during trophoblast differentiation (Fig. 5A).

For the majority of DMRs for which allelic methylation was observed in the somatic tissues (80%), the genomic interval showing methylation differences between sperm and phES cells is larger than the allelic DMRs in hES cells and somatic tissues (Fig. 5B,C). In the case of maternally methylated DMRs, we observe that these regions are flanked by fully methylated intervals in both gametes, and that these DMRs are observed as regions devoid of methylation in the sperm genome. Interrogation of ChIP-seq data sets for nucleosomes containing the histone modifications revealed that the majority of unmethylated DMR regions in sperm are enriched for H3K4me3 containing nucleosome fractions. Our analysis indicates that the size of the unmethylated region in sperm is therefore associated with nucleosome occupancy, rather than protamines. Notably, the maternally methylated germline DMR overlapping the *NNAT* promoter is ~4 kb, as defined by full methylation in phES cell and the H3K4me3 enriched DNA unmethylated region in sperm. This region contracts to an ~1.5-kb region of maternal methylation after preimplantation reprogramming as represented by blastocyst-derived hES cells and somatic tissue profiles (Fig. 5C; Supplemental Fig. S9A showing the contraction at the *NAP1L5* locus). Such resizings are also observed in mouse (Tomizawa et al. 2011), suggesting that imprinted DMRs are not totally protected from genome-wide demethylation during the oocyte to embryo transition. We speculate that the larger regions of differential methylation dictated by the gametes, in combination with protective factors, ensure that they survive reprogramming.

In addition, we also observe other subtle differences in germline-derived methylation profiles. For example, the two sides of the *GNAS-XL* DMR that we show to have independent H3K4 methylation profiles from each other behave differently in the germline, with the *GNAS-AS1* side being a somatic DMR only, but the *GNAS-XL* side being methylated in phES cells and hypomethylated in sperm (Supplemental Fig. S4). Lastly, we identified a dynamic relocalization of methylation at the *FAM50B* DMR during preimplantation development. The 1.2-kb promoter of this imprinted retrogene is methylated on the maternal allele in somatic tissues but is completely unmethylated in phES cells and hES cells derived from six-cell embryos, and has been shown to be unmethylated in sperm (Nakabayashi et al. 2011). However, we do find that allelic methylation is conferred during preimplantation development, at a point between the six-cell stage and blastocyst development. In fact, the ~1-kb regions flanking the promoter (labeled 1 and 3 in Supplemental Fig. S9B) show strongly opposing methylation profiles, with the sperm being unmethylated and phES cells methylated, which then become fully methylated on both alleles immediately after fertilization, leaving allelic methylation over the promoter itself.

Discussion

Differentially methylated regions between the parental alleles are essential for genomic imprinting and development. In this study, we have performed a comprehensive survey of methylation in various human tissues, uncovering all known imprinted DMRs as well as 21 novel loci, which we demonstrate wherever possible regulate imprinted transcription. Our present work demonstrates that the human genome contains a significantly larger number of regions of parent-of-origin methylation than previously thought. The identification of imprinted domains has traditionally been performed in mouse by utilizing gynogenetic and androgenetic embryos, mice harboring regions of uniparental disomies, or highly polymorphic inbred strains (Cooper and Constância 2010). These embryos have been subjected to expression-based screens, including RNA-seq (Gregg et al. 2010; Okae et al. 2011), and genome-wide methylation techniques (Hayashizaki et al. 1994; Kelsey et al. 1999; Hiura et al. 2010). By relying on the confirmation of the evolutionarily conserved expression of the human orthologs, imprinted genes specific to higher primates and humans would have been missed. We have utilized high-throughput bisulfite analysis from in vitro models of gametes and early embryos, and somatic and placental DNA, to characterize the developmental dynamics of imprinted methylation coupled with allelic expression analysis of nearby transcripts. This analysis reveals that 30 regions of parentally inherited differential methylation are observed in humans but not mice. Conversely, we also show that the DMRs associated with *Cdkn1c*, *Rasgrf1*, the *Igf2r* promoter, *Impact*, *Slc38a4*, and *Zrsr1* (previously known as *U2af1-rs1*) imprinted transcripts in mouse do not exhibit allelic methylation in humans (Xie et al. 2012).

Recently, a novel mechanism has been described in which differences in germline methylation can give rise to tissue-specific DMRs in mouse (Proudhon et al. 2012). The *Cdh15* DMR inherits methylation from the oocyte and maintains this parental allelic methylation during in utero development and in adults, with the exception that the paternal allele gains methylation in various brain regions. Therefore, the intragenic *Cdh15* DMR is conserved during adulthood, but in a tissue-specific manner. In humans, the *CDH15* locus does not exhibit allelic DNA methylation in any tissue (data not shown), suggesting that this tissue-specific methylation profile might be limited to mice. We cannot rule out the existence of temporally regulated tissue-specific imprinted DMR in humans, since our samples were derived from adults, and therefore any imprinted DMRs specific to the fetal period would be missed.

Our study reveals the power of combining WGBS and Infinium HumanMethylation450 BeadChip arrays to identify novel imprinted DMRs. We have previously combined reciprocal genome-wide UPD samples and the Infinium HumanMethylation27

Figure 4. The methylation profiles of imprinted loci in placenta compared to somatic tissues. The placenta- and leukocyte-derived WGBS and Infinium array profiles at the (*A*) *PEG10* and (*B*) *H19* loci. Infinium methylation values for normal leukocytes (black dots), with values for the genome-wide pUPD (blue) and mUPD (red) superimposed on the leukocyte WGBS track. Similarly, Infinium methylation values for normal placenta (black dots) and hydatidiform mole (blue dots) are overlaid on the placental WGBS track. The error bars associated with the Infinium array probes represent the standard deviation of multiple biological samples. Bisulfite PCR analysis was used to confirm the tissue-specific methylation profiles. (*C*) Complex tissue-specific allelic methylation and expression patterns at the *ZNF331-MIR512* cluster locus on chromosome 19. The *ZNF331* sequence traces represent the RT-PCR products from leukocytes, whereas both the *MIR512-1* cluster and *MIR371/2* are from placenta. (*D*) A placental-specific imprinted DMR identified using the placenta-derived WGBS and Infinium array data sets. The methylation profiles were confirmed using standard bisulfite PCR on heterozygous DNA samples with allelic RT-PCR performed on placental biopsies. The results confirm that the region of maternal methylation overlapping the *AGBL3* promoter dictates paternal expression of this gene in placenta.

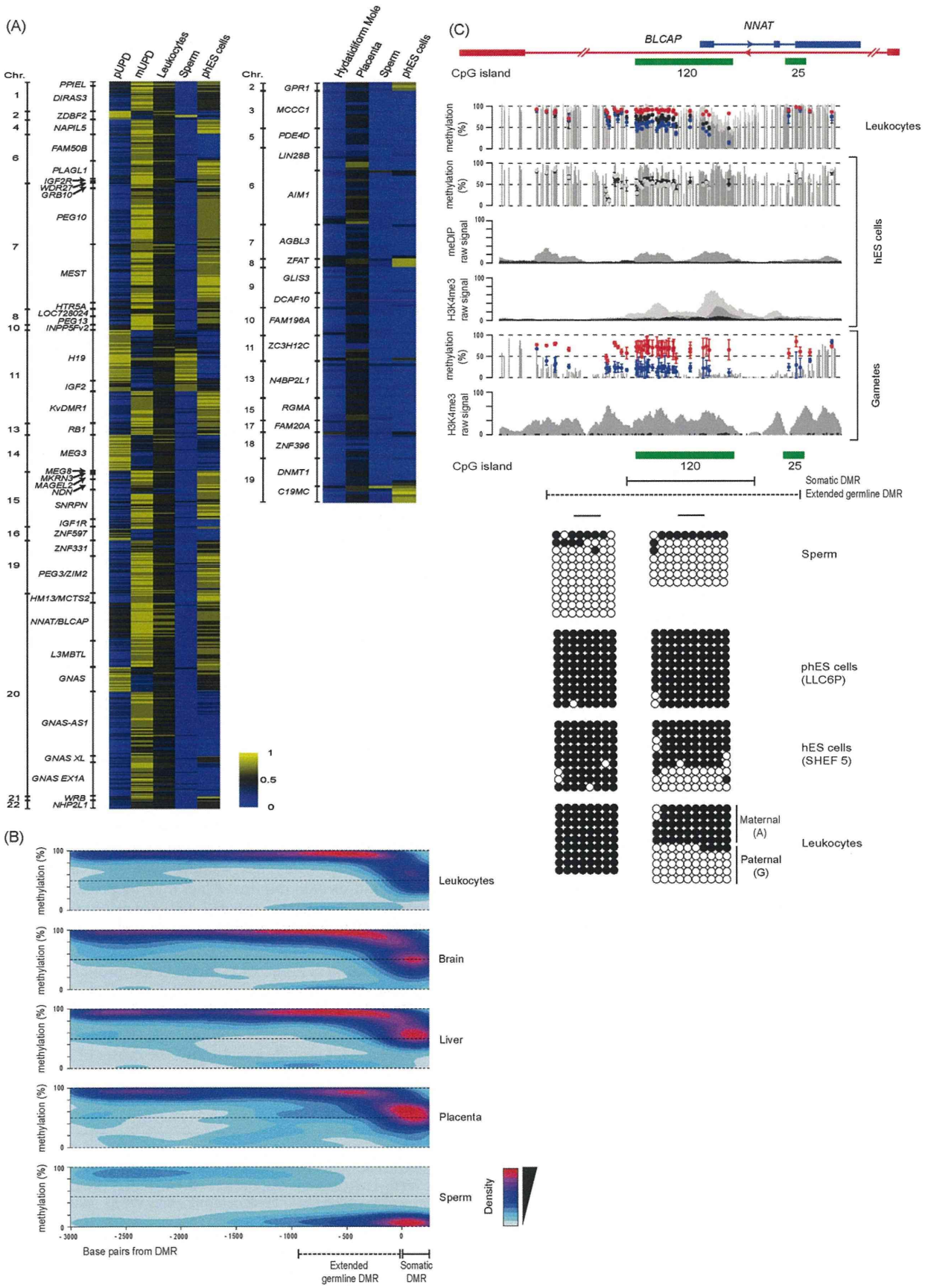

Figure 5. (Legend on next page)

BeadChip arrays to identify imprinted loci (Nakabayashi et al. 2011). All new regions of ubiquitous imprinted methylation identified in the current screen are associated predominantly with type II Infinium probes and were not present on previous array platforms. Of the placental-specific DMRs, only those associated with *DNMT1*, *AIM1*, and *MCCC1* have been previously described (Yuen et al. 2011; Das et al. 2013). Intriguingly, the somatic promoter of *Dnmt1* is differentially methylated between sperm and oocytes but is lost during preimplantation development (Smallwood et al. 2011; Kobayashi et al. 2012). Two of these placental-specific DMRs are associated with type I Infinium probes and were previously discovered using the Infinium HumanMethylation27 BeadChip arrays with DNA derived from diandric and digynic triploid placental samples (Yuen et al. 2011).

Our data provide the first direct evidence in humans that the differential methylation associated with imprinted genes is dynamically regulated upon fusion of the gametes at fertilization. Most maternally methylated DMRs are surrounded by regions of complete methylation in both gametes, and as in mice, the DMRs are clearly observed as unmethylated islands in the sperm genome. These unmethylated intervals are often more extensive in sperm compared to somatic tissues, suggesting that resizing occurs during embryonic transition. It was recently reported that nucleosomes are retained at specific functional regions in sperm chromatin and are refractory to protamine exchange (Hammoud et al. 2009). These sperm-derived histones are enriched for H3K4me3, a permissive modification that is mutually exclusive with DNA methylation, implicating these H3K4me3 regions in the maintenance of the unmethylated state in the male germline.

Imprints are distinguishable from other forms of gametic methylation as they survive the reprogramming that initiates immediately upon fertilization (Smallwood et al. 2011; Kobayashi et al. 2013; Proudhon et al. 2012). By comparing the profiles of sperm, phES, and conventional hES cells along with somatic tissues, we present evidence that most maternally methylated DMRs are not completely refractory to reprogramming, as highlighted by the substantial resizing of the paternally derived unmethylated alleles. These data are consistent with the notion that the cores of imprinted DMRs are protected from Tet-associated demethylation by recruiting heterochromatic factors such as ZFP57 and DPPA3 (also known as STELLA or PGC7) (Nakamura et al. 2007; Li et al. 2008). Similar mechanisms could also act to protect the core of the unmethylated paternal alleles from methylation.

A search for the mouse ZFP57 recognition sequence ($TGCC^{met}GC$) identified numerous binding sites within the ubiquitous imprinted DMRs that may be involved in protecting methylation during preimplantation reprogramming (Quenneville et al. 2011). It is currently unknown if this hexonucleotide motif is bound by ZFP57 in human cells, but patients with mutated ZFP57 lack DNA binding capacity in in vitro EMSA studies (Baglivo et al. 2013).

There are significantly fewer ZFP57 sequence motifs in the placental-specific DMRs compared to the ubiquitous DMRs that inherit methylation from the germline ($P < 0.05$, Student's *t*-test), with 14/17 placental-specific DMRs being unmethylated and not associated with H3K9me3 in hES cells (Supplemental Fig. S10). These data further support our hypothesis that a novel imprinting mechanism occurs in the placenta, which is one of the first examples of methylation-independent epigenetic inheritance in mammals. In support of our observations, Park and colleagues (Park et al. 2004) generated a *H19* ICR knock-in at the *Afp* locus which was de novo methylated around gastrulation, implying that *H19* ICR is differentially marked in the gametes by a mechanism other than methylation. However, it is unknown if this mechanism also occurs at the endogenous *H19* locus. In our examples of placental-specific DMRs, the epigenetic mark inherited from the oocyte is currently unknown, but must be recognized by the de novo methylation machinery during early trophoblast differentiation, since we observe maternal methylation in term placenta. Certain histone methylation states are reported to recruit DNMTs (Dhayalan et al. 2010; Zhang et al. 2010). Since various post-translational modifications of histone tails have been shown to be present at imprinted loci, specifically in the placenta independent of DNA methylation (Umlauf et al. 2004; Monk et al. 2006), we are led to suggest one inviting hypothesis: A histone modification confers the "imprint" at these novel placental-specific imprinted loci. Alternatively, the DNMTs may be recruited to these loci by a specific, yet to be identified, transcription factor expressed during early trophoblast differentiation.

In line with other well-characterized imprinted genes in the placenta, the placental-specific imprinted transcripts may also exert supply-and-demand forces between the developing fetus and mother, ultimately influencing fetal adaptation in utero, which if disrupted may have long-term consequences on health many decades after delivery (Constância et al. 2004). Our observation of imprinting of the somatic promoter of *DNMT1* in placenta may therefore assist in this process. In addition, numerous studies have also suggested that children born as a result of assisted reproductive technologies (ART), including ovarian stimulation, in vitro fertilization, and intra-cytoplasmic sperm injections, have a higher risk of diseases with epigenetic etiologies, including imprinting disorders (Amor and Halliday 2008). In a clinical context, the placenta-specific imprinted loci may be prone to epigenetic instability during ART, as the first differentiation step that results in the trophectoderm occurs when the developing blastocysts are in culture.

By utilizing genome-wide methylation profiling at base-pair resolution, we have catalogued regions of parentally inherited methylation associated with imprinted regions and highlighted all differences between somatic and placental tissues. Further studies of these loci will provide insight into the causes of epigenetic ab-

Figure 5. Methylation in gametes, hES cells, and somatic tissues. (*A*) Heat maps for Infinium probes mapping within all ubiquitous (*left*) and placental-specific (*right*) imprinted DMRs in sperm and phES cells reveal the germline acquisition of methylation. (*B*) Methylation contour plots from WGBS data sets for all maternally methylated DMRs reveal that the extent of the intermediately methylated regions associated with imprinted DMRs are extremely consistent between somatic tissues and significantly larger in sperm. (C) Methylation profiles at the *NNAT* DMR determined by WGBS, Infinium array, and meDIP-seq data sets in leukocytes, sperm, phES cells, and hES cells, along with the H3K4me3 ChIP-seq reads for hES cells and sperm. The gray and black dots in the second panel represent Infinium probe methylation in hES cell lines derived from six-cell blastomeres (Val10B) and blastocytes (SHEF5), respectively. The gametic WGBS methylation profile is derived from sperm, with Infinium probe methylation values for sperm and phES cells represented by blue and red dots. The graphic shows the extent of the differentially methylated regions in somatic tissues and between sperm and phES cells. The error bars associated with the Infinium array probes represent the standard deviation of the two sperm samples and four independent phES cell lines. The H3K4me3 ChIP-seq data is from sperm. The methylation profiles were confirmed using standard bisulfite PCR and sequencing.

errations associated with imprinting disorders and may be relevant to the epigenetic causes of common diseases.

Methods

Tissue samples and cell lines

Peripheral blood was obtained from healthy volunteers or from the umbilical cord of newborns for which we obtained matched placental biopsies. These samples were collected at the Hospital St. Joan De Deu (Barcelona, Spain) and the National Center for Child Health and Development (Tokyo, Japan). All placenta-derived DNA samples were free of maternal DNA contamination based on microsatellite repeat analysis. The brain samples were obtained from BrainNet Europe/Barcelona Brain Bank. Ethical approval for this study was granted by the Institutional Review Boards at the National Center for Child Health and Development (project 234), Saga University (21-5), Hamamatsu University School of Medicine (23-12), Hospital St. Joan De Deu Ethics Committee (35/07), and Bellvitge Institute for Biomedical Research (PR006/08). Written informed consent was obtained from all participants.

The hES (SHEF 3, 5, 6 and Val10B) and parthenogenetically activated oocyte (LLC6P, LLC7P, LLC8P, and LLC9P) cell lines were used because they were epigenetically stable at imprinted loci (with the exception of *NNAT* LOM and *GNAS* GOM in LLC7P; LOM of *PEG3* in Val10B; GOM of *MCTS2P* in SHEF3) and grown as previously described (Harness et al. 2011). Ethical approval for the study of these cells was granted by the Bellvitge Institute for Biomedical Research Ethics Committee (PR096/10) and Comité Ético de Investigación Clínica (CEIC) del Centro de Medicina Regenerativa de Barcelona-CMR[B] (28/2012) and complied with the legal guidelines outlined by the Generalitat de Catalunya El conseller de Slaut.

Wild-type mouse embryos and placentae were produced by crossing C57BL/6 (B) with *Mus musculus molosinus* (JF1) or *Mus musculus castaneous* (C) mice. Mouse work was approved by the Institutional Review Board Committees at the National Center for Child Health and Development (approval number A2010-002). Animal husbandry and breeding were conducted according to the institutional guidelines for the care and the use of laboratory animals. DNA and RNA extractions and cDNA synthesis were carried out as previously described (Monk et al. 2006).

Characterization of the genome-wide UPD samples

Genomic DNA was isolated from two previously described genome-wide paternal UPD cases with BWS features (Romanelli et al. 2011) and two newly identified individuals, at Saga University, as well as one genome-wide maternal UPD with a SRS phenotype (Yamazawa et al. 2010). Each of these cases had undergone extensive molecular characterization to confirm genome-wide UPD status and the extent of mosaicism. We used DNA isolated from lymphocytes, as these samples had minimal contamination of the biparental cell lines. The genome-wide pUPD samples had 9, 11, 9, and 2% biparental contribution, whereas the genome-wide SRS sample had 16%. In addition, four hydatidiform moles were collected by the National Center for Child Health and Development.

Genome-wide methylation profiling

We analyzed six publicly available methylomes, including those derived from CD4+ lymphocytes (GSE31263) (Heyn et al. 2012), brain (GSM913595) (Zeng et al. 2012), the H1 hES cell line (GSM432685, GSM432686, GSM429321, GSM429322, GSM429323), and sperm (GSE30340). In addition, we generated three additional tissue methylomes using WGBS for brain, liver, and placenta. WGBS libraries were generated as previously described (Heyn et al. 2012).

We also generated methylation data sets using the Illumina Infinium HumanMethylation450 BeadChip arrays, which simultaneously quantifies ~2% of all CpG dinucleotides. Bisulfite conversion of 600 ng of DNA was performed according to the manufacturer's recommendations for the Illumina Infinium Assay (EZ DNA methylation kit, Zymo). The bisulfite-converted DNA was used for hybridization following the Illumina Infinium HD methylation protocol at genomic facilities of the Cancer Epigenetics and Biology Program (Barcelona, Spain) or the National Center for Child Health and Development. Data was generated for the genome-wide UPDs (4× pUPD, 1× mUPD), two brain, one liver, one muscle, one pancreas, two sperm, four hydatidiform moles, four term placentae, four phES cell lines, and the four hES lines. In addition, we used three leukocyte data sets from GSE30870.

Data filtering and analysis

For WGBS, the sequence reads were aligned to either strand of the hg19 reference genome using a custom computational pipeline (autosomal CpGs with at least five reads: brain sample, 190,314,071 aligned unique reads, 83% coverage; liver sample, 778,733,789 aligned unique reads, 96.6% coverage; placenta sample, 319,362,653 aligned unique reads, 89.6% coverage). The methylation level of each cytosine within CpG dinucleotides was estimated as the number of reads reporting a C, divided by the total number of reads reporting a C or T. For the identification of intermediately methylated regions associated with imprinted DMRs, we performed a sliding window approach in which the methylation of 25 CpGs was averaged after filtering for repetitive sequences. The location of these sequences was taken from the UCSC sequence browser. An interval was considered partially methylated if the average methylation was $0.25 < \text{mean} \pm 1.5\ \text{SD} < 0.75$.

For the Illumina Infinium HumanMethylation 450 BeadChip array, before analyzing the data, we excluded possible sources of technical biases that could influence results. We applied signal background subtraction, and inter-plate variation was normalized using default control probes in BeadStudio (version 2011.1_Infinium HD). We discarded probes with a detection *P*-value >0.01. We also excluded probes that lacked signal values in one or more of the DNA samples analyzed. In addition, we discarded 16,631 probes as they contained SNPs present in >1% of the population (dbSNP 137). Lastly, prior to screening for novel imprinted DMRs, we excluded all X chromosome CpG sites. In total, we analyzed 442,772 probes in all DNA samples. All hierarchical clustering and β-value evaluation was performed using the Cluster Analysis tool of the BeadStudio software.

In-house R-package scripts were used to evaluate the average methylation of three contiguous Infinium probes. To identify regions with potential allelic methylation, we screened the reciprocal genome-wide UPDs for three consecutive probes with an average β-value difference greater than 0.3 (Limma linear model $P < 0.05$):

$$\left| \frac{1}{3} \sum_{n=0}^{2} pUPDs_n - \frac{1}{3} \sum_{n=0}^{2} mUPD_n \right| > 0.3.$$

With the condition that the average of three consecutive probes for the normal leukocytes is between the values for the reciprocal genome-wide UPDs:

$$\begin{cases} if \frac{1}{3}\sum_{n=0}^{2} pUPDs_n > \frac{1}{3}\sum_{n=0}^{2} mUPD_n \\ then \frac{1}{3}\sum_{n=0}^{2} pUPDs_n > \frac{1}{3}\sum_{n=0}^{2} Leukocytes_n > \frac{1}{3}\sum_{n=0}^{2} mUPD_n \\ if \frac{1}{3}\sum_{n=0}^{2} mUPD_n > \frac{1}{3}\sum_{n=0}^{2} pUPDs_n \\ then \frac{1}{3}\sum_{n=0}^{2} mUPD_n > \frac{1}{3}\sum_{n=0}^{2} Leukocytes_n > \frac{1}{3}\sum_{n=0}^{2} pUPDs_n. \end{cases}$$

The final condition was that the average of three consecutive probes for normal leukocytes is within the 0.25–0.75 intermediate methylation range:

$$0.25 > \frac{1}{3}\sum_{n=0}^{2} Leukocytes_n > 0.75.$$

Genotyping and imprinting analysis

Genotypes of potential SNPs identified in the UCSC Genome Browser (hg19) were obtained by PCR and direct sequencing. Sequence traces were interrogated using Sequencher v4.6 (Gene Codes Corporation) to distinguish heterozygous and homozygous samples. Heterozygous sample sets were analyzed for either allelic expression using RT-PCR or bisulfite PCR, incorporating the polymorphism within the final PCR amplicon so that parental alleles could be distinguished (for primer sequence, see Supplemental Table S3).

Bisulfite PCR

Approximately 1 μg DNA was subjected to sodium bisulfite treatment and purified using the EZ DNA Methylation-Gold kit (Zymo), and was used for all bisulfite PCR analysis. Approximately 2 μL of bisulfite-converted DNA was used in each amplification reaction using Immolase Taq polymerase (Bioline) at 35–45 cycles, and the resulting PCR product cloned into pGEM-T easy vector (Promega) for subsequent subcloning and sequencing (for primer sequence, see Supplemental Table S3). For the confirmation of an imprinted DMR, we analyzed a minimum of three heterozygous samples and, where possible, two different tissues.

Chromatin immunoprecipitation (ChIP)

We analyzed publicly available H3K4me3 ChIP-seq and meDIP-seq data sets, including those derived from lymphocytes (GSM772948, GSM772836, GSM772916, GSM543025, GSM613913), brain (GSM806943, GSM806935, GSM806948, GSM669614, GSM669615), and the H1 hES cell line (GSM409308, GSM469971, GSM605315, GSM428289, GSM456941, GSM543016). For H3K9me3 in hES cells, we used GSM450266. In addition, we used the sperm ChIP-seq data set for H3K4me3 as a direct measure of nucleosome occupancy (GSM392696, GSM392697, GSM392698, GSM392714, GSM392715, GSM392716) (Hammoud et al. 2009).

The confirmation of allelic H3K4me3 in leukocytes or lymphoblastoid cell lines was performed as previously described (Iglesias-Platas et al. 2013). Briefly, 100 μg of chromatin was used for an immunoprecipitation reaction with Protein A agarose/salmon sperm DNA (16-157, Millipore) and a H3K4me3 (07-473, Millipore). Each ChIP was performed in triplicate alongside a mock immunoprecipitation with an unrelated IgG antiserum, and a 1% fraction of the input chromatin was extracted in parallel. Levels of immunoprecipitated chromatin at each specific region were determined by qPCR using SYBR Green (Applied Biosystems) carried out on the Applied Biosystems 7900 Fast real-time PCR system (for primer sequence, see Supplemental Table S3). Each PCR was run in triplicate and protein binding was quantified as a percentage of total input material.

Data access

The data from this study have been submitted to the NCBI Gene Expression Omnibus (GEO; http://www.ncbi.nlm.nih.gov/geo/) under accession number GSE52578.

List of affiliations

[1]Imprinting and Cancer Group, Cancer Epigenetic and Biology Program, Institut d'Investigació Biomedica de Bellvitge, Hospital Duran i Reynals, 08908 Barcelona, Spain; [2]Department of Maternal-Fetal Biology, National Research Institute for Child Health and Development, Tokyo 157-8535, Japan; [3]Servicio de Neonatología, Hospital Sant Joan de Déu, Fundació Sant Joan de Déu, 08950 Barcelona, Spain; [4]Department of Systems Biomedicine, National Research Institute for Child Health and Development, Tokyo 157-8535, Japan; [5]Fundación IVI-Instituto Universitario IVI-Universidad de Valencia, INCLIVA, 46980 Paterna, Valencia, Spain; [6]Centre for Stem Cell Biology, Department of Biomedical Science, University of Sheffield, Sheffield S10 2TN, United Kingdom; [7]Reeve-Irvine Research Centre, Sue and Bill Gross Stem Cell Research Center, Department of Anatomy and Neurobiology, School of Medicine, University of California at Irvine, Irvine, California 92697, USA; [8]Cancer Epigenetics Group, Cancer Epigenetic and Biology Program, Institut d'Investigació Biomedica de Bellvitge, Hospital Duran i Reynals, 08908 Barcelona, Spain; [9]Department of Obstetrics and Gynecology, Graduate School of Medical Science, Kyushu University, Fukuoka 812-8582, Japan; [10]Instituto de Genética Médica y Molecular, CIBERER, IDIPAZ-Hospital Universitario La Paz, Universidad Autónoma de Madrid, 28046 Madrid, Spain; [11]Division of Molecular Genetics and Epigenetics, Department of Biomolecular Sciences, Faculty of Medicine, Saga University, Saga 849-8501, Japan; [12]Department of Physiological Sciences II, School of Medicine, University of Barcelona, 08036 Barcelona, Catalonia, Spain; [13]Institucio Catalana de Recerca i Estudis Avançats (ICREA), 08010 Barcelona, Catalonia, Spain; [14]Department of Pediatrics, Hamamatsu University School of Medicine, Hamamatsu 431-3192, Japan.

Acknowledgments

We thank S. Morán at PEBC-IDIBELL for performing the methylation array hybridization and S. Sayols and H. Heyn for bioinformatics assistance. We also thank P. Arnaud and J. Frost for stimulating discussions and helpful comments. This work was partially funded by grants from the Fundació La Marató de TV3 (grant no. 101130 to D.M. and P.L.); Spanish Ministerio de Educacion y Ciencia (BFU2011-27658 to D.M.); JST/CREST and the Health and Labour Sciences Research Grant (Nanbyo-Ippan-003 to K.H.); the Ministry of Education, Culture, Sports, Science, and Technology of Japan (#22249010) and the National Center for Child Health and Development (#24-3) to K.N. D.M. is a Ramon y Cajal research fellow. Finally, we would like to thank all the patients and their families for participating in this project.

References

Amor DJ, Halliday J. 2008. A review of known imprinting syndromes and their association with assisted reproduction technologies. *Hum Reprod* **23:** 2826–2834.

Baglivo I, Esposito S, De Cesare L, Sparago A, Anvar Z, Riso V, Cammisa M, Fattorusso R, Grimaldi G, Riccio A, et al. 2013. Genetic and epigenetic mutations affect the DNA binding capability of human ZFP57 in transient neonatal diabetes type 1. *FEBS Lett* **587:** 1474–1481.
Barbaux S, Gascoin-Lachambre G, Buffat C, Monnier P, Mondon F, Tonanny MB, Pinard A, Auer J, Bessières B, Barlier A, et al. 2012. A genome-wide approach reveals novel imprinted genes expressed in the human placenta. *Epigenetics* **7:** 1079–1090.
Bourc'his D, Xu GL, Lin CS, Bollman B, Bestor TH. 2001. Dnmt3L and the establishment of maternal genomic imprints. *Science* **294:** 2536–2539.
Buiting K. 2010. Prader-Willi syndrome and Angelman syndrome. *Am J Med Genet C Semin Med Genet* **154C:** 365–376.
Choufani S, Shuman C, Weksberg R. 2010. Beckwith-Wiedemann syndrome. *Am J Med Genet C Semin Med Genet* **154C:** 343–354.
Ciccone DN, Su H, Hevi S, Gay F, Lei H, Bajko J, Xu G, Li E, Chen T. 2009. KDM1B is a histone H3K4 demethylase required to establish maternal genomic imprints. *Nature* **461:** 415–418.
Constância M, Kelsey G, Reik W. 2004. Resourceful imprinting. *Nature* **432:** 53–57.
Coombes C, Arnaud P, Gordon E, Dean W, Coar EA, Williamson CM, Feil R, Peters J, Kelsey G. 2003. Epigenetic properties and identification of an imprint mark in the Nesp-Gnasxl domain of the mouse *Gnas* imprinted locus. *Mol Cell Biol* **23:** 5475–5488.
Cooper WN, Constância M. 2010. How genome-wide approaches can be used to unravel the remaining secrets of the imprintome. *Brief Funct Genomics* **9:** 315–328.
Das R, Lee YK, Strogantsev R, Jin S, Lim YC, Ng PY, Lin XM, Chng K, Yeo GSh, Ferguson-Smith AC, et al. 2013. DNMT1 and AIM1 imprinting in human placenta revealed through a genome-wide screen for allele-specific DNA methylation. *BMC Genomics* **14:** 685.
Dhayalan A, Rajavelu A, Rathert P, Tamas R, Jurkowska RZ, Ragozin S, Jeltsch A. 2010. The Dnmt3a PWWP domain reads histone 3 lysine 36 trimethylation and guides DNA methylation. *J Biol Chem* **285:** 26114–26120.
Eggermann T. 2010. Russell-Silver syndrome. *Am J Med Genet C Semin Med Genet* **154C:** 355–364.
Ehrlich M, Gama-Sosa MA, Huang LH, Midgett RM, Kuo KC, McCune RA, Gehrke C. 1982. Amount and distribution of 5-methylcytosine in human DNA from different types of tissues of cells. *Nucleic Acids Res* **10:** 2709–2721.
El-Maarri O, Buiting K, Peery EG, Kroisel PM, Balaban B, Wagner K, Urman B, Heyd J, Lich C, Brannan CI, et al. 2001. Maternal methylation imprints on human chromosome 15 are established during or after fertilization. *Nat Genet* **27:** 41–44.
Fuke C, Shimabukuro M, Petronis A, Sugimoto J, Oda T, Miura K, Miyazaki T, Ogura C, Okazaki Y, Jinno Y. 2004. Age related changes in 5-methylcytosine content in human peripheral leukocytes and placentas: An HPLC-based study. *Ann Hum Genet* **68:** 196–204.
Geuns E, De Temmerman N, Hilven P, Van Steirteghem A, Liebaers I, De Rycke M. 2007. Methylation analysis of the intergenic differentially methylated region of DLK1-GTL2 in human. *Eur J Hum Genet* **15:** 352–361.
Gregg C, Zhang J, Weissbourd B, Luo S, Schroth GP, Haig D, Dulac C. 2010. High-resolution analysis of parent-of-origin allelic expression in the mouse brain. *Science* **329:** 643–648.
Hammoud SS, Nix DA, Zhang H, Purwar J, Carrell DT, Cairns BR. 2009. Distinctive chromatin in human sperm packages genes for embryo development. *Nature* **460:** 473–478.
Harness JV, Turovets NA, Seiler MJ, Nistor G, Altun G, Agapova LS, Ferguson D, Laurent LC, Loring JF, Keirstead HS. 2011. Equivalence of conventionally-derived and parthenote-derived human embryonic stem cells. *PLoS ONE* **6:** e14499.
Hata K, Okano M, Lei H, Li E. 2002. Dnmt3L cooperates with the Dnmt3 family of de novo DNA methyltransferases to establish maternal imprints in mice. *Development* **129:** 1983–1993.
Hayashizaki Y, Shibata H, Hirotsune S, Sugino H, Okazaki Y, Sasaki N, Hirose K, Imoto H, Okuizumi H, Muramatsu M, et al. 1994. Identification of an imprinted U2af binding protein related sequence on mouse chromosome 11 using the RLGS method. *Nat Genet* **6:** 33–40.
Heyn H, Li N, Ferreira HJ, Moran S, Pisano DG, Gomez A, Diez J, Sanchez-Mut JV, Setien F, Carmona FJ, et al. 2012. Distinct DNA methylomes of newborns and centenarians. *Proc Natl Acad Sci* **109:** 10522–10527.
Hiura H, Sugawara A, Ogawa H, John RM, Miyauchi N, Miyanari Y, Horiike T, Li Y, Yaegashi N, Sasaki H, et al. 2010. A tripartite paternally methylated region within the *Gpr1-Zdbf2* imprinted domain on mouse chromosome 1 identified by meDIP-on-chip. *Nucleic Acids Res* **38:** 4929–4945.
Kanber D, Berulava T, Ammerpohl O, Mitter D, Richter J, Siebert R, Horsthemke B, Lohman D, Buiting K. 2009. The human retinoblastoma gene is imprinted. *PLoS Genet* **12:** e1000790.
Iglesias-Platas I, Court F, Camprubi C, Sparago A, Guillaumet-Adkins A, Martin-Trujillo A, Riccio A, Moore GE, Monk D. 2013. Imprinting at the *PLAGL1* domain is contained within a 70-kb CTCF/cohesin-mediated non-allelic chromatin loop. *Nucleic Acids Res* **41:** 2171–2179.
Kagami M, Sekita Y, Nishimura G, Irie M, Kato F, Okada M, Yamamori S, Kishimoto H, Nakayama M, Tanaka Y, et al. 2008. Deletions and epimutations affecting the human 14q32.2 imprinted region in individuals with paternal and maternal upd(14)-like phenotypes. *Nat Genet* **40:** 237–242.
Kagami M, O'Sullivan MJ, Green AJ, Watabe Y, Arisaka O, Masawa N, Matsuoka K, Fukami M, Matsubara K, Kato F, et al. 2010. The IG-DMR and the *MEG3*-DMR at human chromosome 14q32.2: Hierarchical interaction and distinct functional properties as imprinting control centers. *PLoS Genet* **6:** e1000992.
Kelsey G. 2010. Imprinting on chromosome 20: Tissue-specific imprinting and imprinting mutations in the GNAS locus. *Am J Med Genet C Semin Med Genet* **154C:** 377–386.
Kelsey G, Bodle D, Miller HJ, Beechey CV, Coombes C, Peters J, Williamson CM. 1999. Identification of imprinted loci by methylation-sensitive representational difference analysis: Application to mouse distal chromosome 2. *Genomics* **62:** 129–138.
Kobayashi H, Sakurai T, Imai M, Takahashi N, Fukuda A, Yayoi O, Sato S, Nakabayashi K, Hata K, Sotomaru Y, et al. 2012. Contribution of intragenic DNA methylation in mouse gametic DNA methylomes to establish oocyte-specific heritable marks. *PLoS Genet* **8:** e1002440.
Kobayashi H, Yanagisawa E, Sakashita A, Sugawara N, Kumakura S, Ogawa H, Akutsu H, Hata K, Nakabayashi K, Kono T. 2013. Epigenetic and transcriptional features of the novel human imprinted lncRNA *GPR1AS* suggest it is a functional ortholog to mouse *Zdbf2linc*. *Epigenetics* **8:** 635–645.
Kong A, Steinthorsdottir V, Masson G, Thorleifsson G, Sulem P, Besenbacher S, Jonasdottir A, Sigurdsson A, Kristinsson KT, Jonasdottir A, et al. 2009. Parental origin of sequence variants associated with complex diseases. *Nature* **462:** 868–874.
Lapunzina P, Monk D. 2011. The consequences of uniparental disomy and copy number neutral loss-of-heterozygosity during human development and cancer. *Biol Cell* **103:** 303–317.
Li X, Ito M, Zhou F, Youngson N, Zuo X, Leder P, Ferguson-Smith AC. 2008. A maternal-zygotic effect gene, *Zfp57*, maintains both maternal and paternal imprints. *Dev Cell* **15:** 547–557.
Lister R, Pelizzola M, Dowen RH, Hawkins RD, Hon G, Tonti-Filippini J, Nery JR, Lee L, Ye Z, Ngo QM, et al. 2009. Human DNA methylomes at base resolution show widespread epigenomic differences. *Nature* **462:** 315–322.
Lopes S, Lewis A, Hajkova P, Dean W, Oswald J, Forné T, Murrell A, Constância M, Bartolomei M, Walter J, et al. 2003. Epigenetic modifications in an imprinting cluster are controlled by a hierarchy of DMRs suggesting long-range chromatin interactions. *Hum Mol Genet* **12:** 295–305.
Mackay DJ, Temple IK. 2010. Transient neonatal diabetes mellitus type 1. *Am J Med Genet C Semin Med Genet* **154C:** 335–342.
Mai Q, Yu Y, Li T, Wang L, Chen MJ, Huang SZ, Zhou C, Zhou Q. 2007. Derivation of human embryonic stem cell lines from parthenogenetic blastocysts. *Cell Res* **17:** 1008–1012.
Molaro A, Hodges E, Fang F, Song Q, McCombie WR, Hannon GJ, Smith AD. 2011. Sperm methylation profiles reveal features of epigenetic inheritance and evolution in primates. *Cell* **146:** 1029–1041.
Monk D. 2010. Deciphering the cancer imprintome. *Brief Funct Genomics* **9:** 329–339.
Monk D, Arnaud P, Apostolidou S, Hills FA, Kelsey G, Stanier P, Feil R, Moore GE. 2006. Limited evolutionary conservation of imprinting in the human placenta. *Proc Natl Acad Sci* **103:** 6623–6628.
Nakabayashi K, Trujillo AM, Tayama C, Camprubi C, Yoshida W, Lapunzina P, Sanchez A, Soejima H, Aburatani H, Nagae G, et al. 2011. Methylation screening of reciprocal genome-wide UPDs identifies novel human-specific imprinted genes. *Hum Mol Genet* **20:** 3188–3197.
Nakamura T, Arai Y, Umehara H, Masuhara M, Kimura T, Taniguchi H, Sekimoto T, Ikawa M, Yoneda Y, Okabe M. 2007. PGC7/Stella protects against DNA demethylation in early embryogenesis. *Nat Cell Biol* **9:** 64–71.
Noguer-Dance M, Abu-Amero S, Al-Khtib M, Lefèvre A, Coullin P, Moore GE, Cavaillé J. 2010. The primate-specific microRNA gene cluster (C19MC) is imprinted in the placenta. *Hum Mol Genet* **19:** 3566–3582.
Okae H, Hiura H, Nishida Y, Funayama R, Tanaka S, Chiba H, Yaegashi N, Nakayama K, Sasaki H, Arima T. 2011. Re-investigation and RNA sequencing-based identification of genes with placenta-specific imprinted expression. *Hum Mol Genet* **21:** 548–558.
Park KY, Sellars EA, Grinberg A, Huang SP, Pfeifer K. 2004. The H19 differentially methylated region marks the parental origin of a heterologous locus without gametic DNA methylation. *Mol Cell Biol* **24:** 3588–3595.
Proudhon C, Duffié R, Ajjan S, Cowley M, Iranzo J, Carbajosa G, Saadeh H, Holland ML, Oakey RJ, Rakyan VK, et al. 2012. Protection against de

novo methylation is instrumental in maintaining parent-of-origin methylation inherited from the gametes. *Mol Cell* **47:** 909–920.
Quenneville S, Verde G, Corsinotti A, Kapopoulou A, Jakobsson J, Offner S, Baglivo I, Pedone PV, Grimaldi G, Riccio A, et al. 2011. In embryonic stem cells, ZFP57/KAP1 recognize a methylated hexanucleotide to affect chromatin and DNA methylation of imprinting control regions. *Mol Cell* **44:** 361–372.
Ramowitz LK, Bartolomei MS. 2011. Genomic imprinting: Recognition and marking of imprinted loci. *Curr Opin Genet Dev* **22:** 72–78.
Romanelli V, Nevado J, Fraga M, Trujillo AM, Mori MÁ, Fernández L, Pérez de Nanclares G, Martínez-Glez V, Pita G, Meneses H, et al. 2011. Constitutional mosaic genome-wide uniparental disomy due to diploidisation: An unusual cancer-predisposing mechanism. *J Med Genet* **48:** 212–216.
Schroeder DI, Blair JD, Lott P, Yu HO, Hong D, Crary F, Ashwood P, Walker C, Korf I, Robinson WP, et al. 2013. The human placenta methylome. *Proc Natl Acad Sci* **110:** 6037–6042.
Sharp A, Migliavacca E, Dupre Y, Stathaki E, Reza Sailani M, Baumer A, Schinzel A, Mackay DJ, Robinson DO, Cobellis G, et al. 2010. Methylation profiling in individuals with uniparental disomy identify novel differentially methylated regions on chromosome 15. *Genome Res* **20:** 1271–1278.
Smallwood SA, Tomizawa S, Krueger F, Ruf N, Carli N, Segonds-Pichon A, Sato S, Hata K, Andrews SR, Kelsey G. 2011. Dynamic CpG island methylation landscape in oocytes and pre-implantation embryos. *Nat Genet* **43:** 811–814.
Smith ZD, Chan MM, Mikkelsen TS, Gu H, Gnirke A, Regev A, Meissner A. 2012. A unique regulatory phase of DNA methylation in the early mammalian embryo. *Nature* **484:** 339–344.
Thomson JP, Skene PJ, Selfridge J, Clouaire T, Guy J, Webb S, Kerr AR, Deaton A, Andrews R, James KD, et al. 2010. CpG islands influence chromatin structure via the CpG-binding protein Cfp1. *Nature* **464:** 1082–1086.
Tomizawa S, Kobayashi H, Watanabe T, Andrews S, Hata K, Kelsey G, Sasaki H. 2011. Dynamic stage-specific changes in imprinted differentially methylated regions during early mammalian development and prevalence of non-CpG methylation in oocytes. *Development* **138:** 811–820.
Umlauf D, Goto Y, Cao R, Cerqueira F, Wagschal A, Zhang Y, Feil R. 2004. Imprinting along the *Kcnq1* domain on mouse chromosome 7 involves repressive histone methylation and recruitment of Polycomb group complexes. *Nat Genet* **36:** 1296–1300.
Wood AJ, Schulz R, Woodfine K, Koltowska K, Beechey CV, Peters J, Bourc'his D, Oakey RJ. 2008. Regulation of alternative polyadenylation by genomic imprinting. *Genes Dev* **22:** 1141–1146.
Xie W, Barr CL, Kim A, Yue F, Lee AY, Eubanks J, Dempster EL, Ren B. 2012. Base-resolution analyses of sequence and parent-of-origin dependent DNA methylation in the mouse genome. *Cell* **148:** 816–831.
Yamazawa K, Nakabayashi K, Kagami M, Sato T, Saitoh S, Horikawa R, Hizuka N, Ogata T. 2010. Parthenogenetic chimaerism/mosaicism with a Silver-Russell syndrome-like phenotype. *J Med Genet* **47:** 782–785.
Yuen RKC, Jiang R, Penaherrera M, McFadeen DE, Robinson WP. 2011. Genome-wide mapping of imprinted differentially methylated regions by DNA methylation profiling of human placentas from triploidies. *Epigenetics & Chromatin* **4:** 10.
Zeng J, Konopka G, Hunt BG, Preuss TM, Geschwind D, Yi SV. 2012. Divergent whole-genome methylation maps of human and chimpanzee brains reveal epigenetic basis of human regulatory evolution. *Am J Hum Genet* **91:** 455–465.
Zhang Y, Jurkowska R, Soeroes S, Rajavelu A, Dhayalan A, Bock I, Rathert P, Brandt O, Reinhardt R, Fischle W, et al. 2010. Chromatin methylation activity of Dnmt3a and Dnmt3a/3L is guided by interaction of the ADD domain with the histone H3 tail. *Nucleic Acids Res* **38:** 4246–4253.

Received August 9, 2013; accepted in revised form December 26, 2013.

CLINICAL GENETICS An International Journal of Genetics, Molecular and Personalized Medicine

Clin Genet 2014: 86: 539–544
Printed in Singapore. All rights reserved

CLINICAL GENETICS
doi: 10.1111/cge.12318

Short Report

A novel *de novo* point mutation of the OCT-binding site in the *IGF2/H19*-imprinting control region in a Beckwith–Wiedemann syndrome patient

Higashimoto K., Jozaki K., Kosho T., Matsubara K., Fuke T., Yamada D., Yatsuki H., Maeda T., Ohtsuka Y., Nishioka K., Joh K., Koseki H., Ogata T., Soejima H. A novel *de novo* point mutation of the OCT-binding site in the *IGF2/H19*-imprinting control region in a Beckwith–Wiedemann syndrome patient.
Clin Genet 2014: 86: 539–544. © John Wiley & Sons A/S. Published by John Wiley & Sons Ltd, 2013

The *IGF2/H19*-imprinting control region (ICR1) functions as an insulator to methylation-sensitive binding of CTCF protein, and regulates imprinted expression of *IGF2* and *H19* in a parental origin-specific manner. ICR1 methylation defects cause abnormal expression of imprinted genes, leading to Beckwith–Wiedemann syndrome (BWS) or Silver–Russell syndrome (SRS). Not only ICR1 microdeletions involving the CTCF-binding site, but also point mutations and a small deletion of the OCT-binding site have been shown to trigger methylation defects in BWS. Here, mutational analysis of ICR1 in 11 BWS and 12 SRS patients with ICR1 methylation defects revealed a novel *de novo* point mutation of the OCT-binding site on the maternal allele in one BWS patient. In BWS, all reported mutations and the small deletion of the OCT-binding site, including our case, have occurred within repeat A2. These findings indicate that the OCT-binding site is important for maintaining an unmethylated status of maternal ICR1 in early embryogenesis.

Conflict of interest

The authors have no competing financial interests to declare.

K. Higashimoto[a], K. Jozaki[a], T. Kosho[b], K. Matsubara[c], T. Fuke[c], D. Yamada[d], H. Yatsuki[a], T. Maeda[a], Y. Ohtsuka[a], K. Nishioka[a], K. Joh[a], H. Koseki[d], T. Ogata[e] and H. Soejima[a]

[a]Division of Molecular Genetics & Epigenetics, Department of Biomolecular Sciences, Faculty of Medicine, Saga University, Saga, Japan, [b]Department of Medical Genetics, Shinshu University School of Medicine, Matsumoto, Nagano, Japan, [c]Department of Molecular Endocrinology, National Research Institute for Child Health and Development, Tokyo, Japan, [d]Laboratory for Developmental Genetics, RIKEN Center for Integrative Medical Sciences (IMS), Yokohama, Kanagawa, Japan, and [e]Department of Pediatrics, Hamamatsu University School of Medicine, Hamamatsu, Japan

Key words: Beckwith–Wiedemann syndrome – ICR1 methylation defect – *IGF2/H19* – OCT-binding site – Silver–Russell syndrome

Corresponding author: Hidenobu Soejima, Division of Molecular Genetics & Epigenetics, Department of Biomolecular Sciences, Faculty of Medicine, Saga University, 5-1-1 Nabeshima, Saga 849–8501, Japan.
Tel.: +81 952 34 2260;
fax: +81 952 34 2067;
e-mail: soejimah@cc.saga-u.ac.jp

Received 5 August 2013, revised and accepted for publication 6 November 2013

Human 11p15 contains two neighboring imprinted domains, *IGF2/H19* and *KCNQ1*. Each domain is controlled by its own imprinting control region: ICR1 or ICR2, respectively (1). ICR1 methylation defects cause abnormal imprinted expression of insulin-like growth factor 2 (*IGF2*), which encodes a growth factor, and non-coding RNA *H19*, which possesses possible tumor-suppressor functions, leading to Beckwith–Wiedemann syndrome (BWS: OMIM 130650) and Silver–Russell syndrome (SRS: OMIM 180860), respectively (1, 2).

BWS is a congenital overgrowth disorder characterized by macroglossia, macrosomia, and abdominal wall defects, whereas SRS is a congenital growth retardation disorder characterized by a typical facial gestalt, clinodactyly V, and body asymmetry (1, 2). Among varied causative genetic and epigenetic abnormalities, ICR1 methylation defects are etiologies common to both diseases. Gain of methylation (GOM) and loss of methylation (LOM) at ICR1 account for ~5% of BWS and ~44% of SRS cases, respectively (1, 2).

ICR1 upstream of *H19* is a differentially methylated region (DMR) that is methylated exclusively on the paternal allele, and it regulates the imprinted expression of paternally expressed *IGF2* and maternally expressed *H19*. On the maternal allele, unmethylated ICR1 bound by CTCF forms a chromatin insulator that prevents *IGF2* promoter activation by the enhancer downstream of *H19*, resulting in silencing of *IGF2* and activation of *H19*. On the paternal allele, methylation-sensitive CTCF cannot bind to methylated ICR1, resulting in activation of *IGF2* and silencing of *H19* (3, 4). CTCF also maintains the unmethylated status of ICR1 on the maternal allele (5, 6).

Human ICR1 contains two different repetitive sequences (A and B) and seven CTCF-binding sites (CTSs) (Fig. 1a). A maternally inherited ICR1 microdeletion (1.4–2.2 kb), which affects ICR1 function and CTCF binding by changing CTS spacing, has been reported to result in ICR1-GOM in a few familial BWS cases (7–9). ICR1 also contains other protein-binding motifs, such as OCT, SOX, and ZFP57 (10, 11). Recently, point mutations and a small deletion of the OCT or SOX motif have been reported in a few BWS patients with ICR1-GOM (10, 12, 13).

Here, mutational analysis in 11 BWS and 12 SRS patients with ICR1 methylation defects revealed a novel *de novo* point mutation in the OCT-binding site on the maternal allele of one BWS patient.

Materials and methods

Patients

Eleven BWS and twelve SRS patients, who were clinically diagnosed, were enrolled in this study. All BWS and SRS patients displayed isolated GOM and LOM of ICR1, respectively. This study was approved by the Ethics Committee for Human Genome and Gene Analyses of the Faculty of Medicine, Saga University. Written informed consents were obtained from the parents or guardians of the patients.

Sequencing analysis of ICR1

A genomic region in and around ICR1, which included seven CTSs and three OCT-binding sites, was directly sequenced in all patients as previously described (14). All polymerase chain reaction (PCR) primer pairs used are listed in Table S1, Supporting Information.

Microsatellite analysis

For quantitative polymorphism analysis, tetranucleotide repeat markers, *D11S1984* at 11p15.5 and *D11S1997* at 11p15.4, were amplified and analyzed with GeneMapper software. The peak height ratios of the paternal allele to the maternal allele were calculated.

Southern blot analysis

Methylation-sensitive Southern blots with *Pst*I/*Mlu*I and *Bam*HI/*Not*I were employed for ICR1 and ICR2, respectively, as described previously (15). Band intensity was measured using a FLA-7000 fluoro-image analyzer (Fujifilm, Tokyo, Japan). The methylation index (MI, %) was then calculated.

Bisulfite sequencing

Bisulfite sequencing was performed covering the three variants within ICR1 that were found in BWS-s043. Genomic DNA was bisulfite-converted using an EpiTect Bisulfite Kit (Qiagen, Hilden, Germany). After PCR amplification, the products were cloned and sequenced.

Electrophoretic mobility shift assay

The pCMX-Flag-human OCT4 and pCMX-Flag-human SOX2 were simultaneously transfected into HEK293 cells. The nuclear extracts from HEK293 cells expressing human OCT4/SOX2 and mouse ES cells were used. Electrophoretic mobility shift assay (EMSA) was performed as described previously (10). For supershift analysis, 1.5 μg of anti-OCT4 antibody (Abcam, ab19857, Cambridge, UK) or 1.5 μg of anti-SOX2 antibody (R&D systems, AF2018, Minneapolis, MN) was used. The unlabeled probes were also used as competitors. The reaction mixtures were separated on a 4% polyacrylamide gel and exposed to a film. Oligonucleotide sequences are presented in Table S1.

Results

Among 11 BWS and 12 SRS patients with ICR1 methylation defects, 7 and 2 variants from 5 BWS and 2 SRS patients were found, respectively (Table 1). The variants in BWS-047 and BWS-s061 were polymorphisms. The remaining variants were not found in the normal population, the UCSC Genome Browser database, or the 1000 Genomes database, suggesting them to be candidates for causative mutations for ICR1 methylation defects. However, the positions of the variants, except

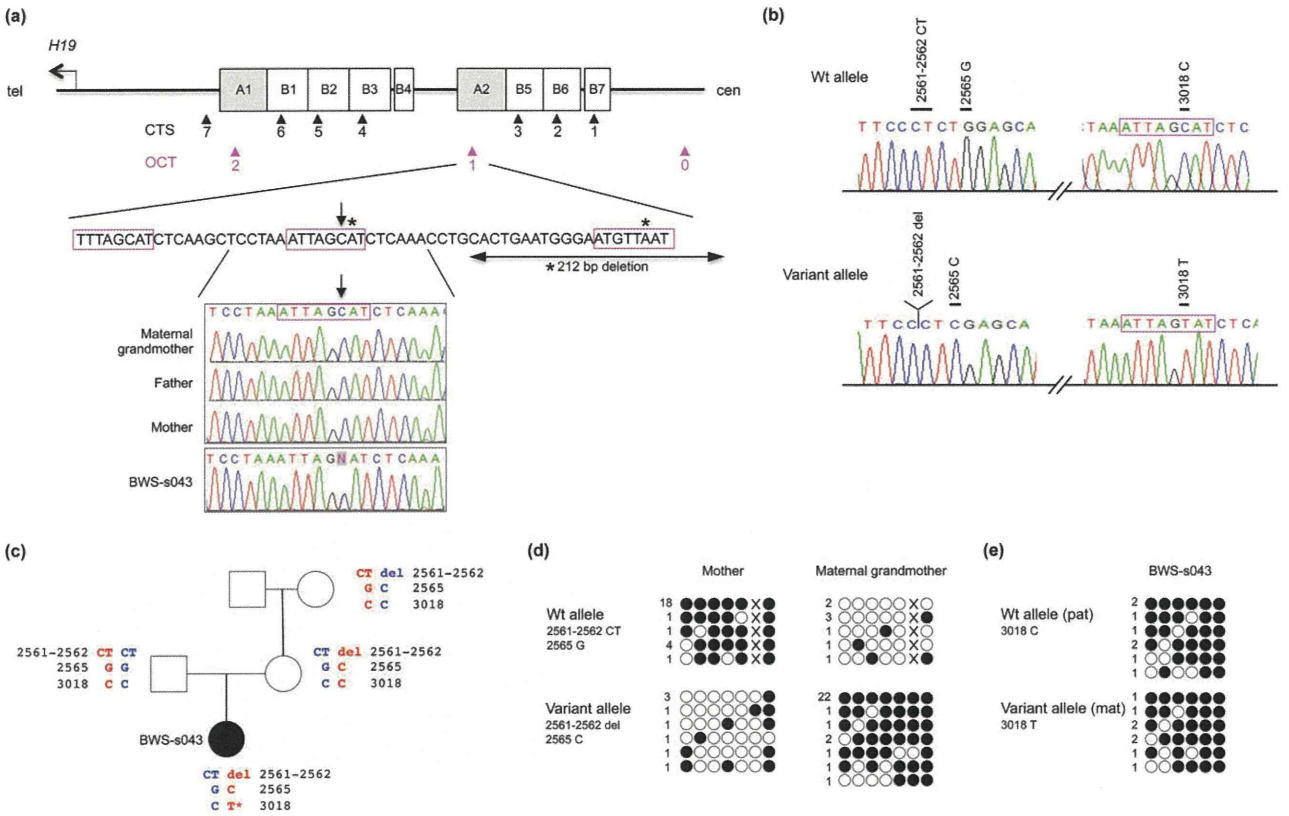

Fig. 1. The three variants in BWS-s043 and their effects on ICR1 methylation. (**a**) Map of ICR1 and the position of 2,023,018C>T. Upper panel: structure of ICR1. ICR1 consists of two repeat blocks. Each block consists of one repeat A and three or four repeat Bs. The black and red arrowheads indicate CTCF-binding sites (CTS) and OCT-binding sites (OCT), respectively. Middle panel: the position of 2,023,018C>T (arrow) and previously reported mutations and deletions (asterisks). Three octamer motifs are enclosed by a red line. Lower panel: electrophoretograms around 2,023,018C>T. BWS-s043 were heterozygous for the variant, whereas the maternal grandmother and both parents did not harbor it. (**b**) Haplotype encompassing the three variants in BWS-s043. Polymerase chain reaction (PCR) products encompassing the three variants were cloned and sequenced. All three variants were revealed to be on the same allele in BWS-s043. (**c**) Pedigree and haplotype of the family. Haplotype analysis showed that 2,023,018C>T (asterisk) occurred on the maternal allele in BWS-s043. (**d**) Bisulfite sequencing analysis encompassing the 2,022,561-562CT>delCT and the 2,022,565G>C variants in the mother and the maternal grandmother. Open and filled circles indicate unmethylated and methylated CpG sites, respectively. X indicates G at chr11: 2,022,565. Numerals on the left reflect the number of clones with the same methylation pattern. The variant allele was unmethylated in the mother and methylated in the maternal grandmother, respectively. (**e**) Bisulfite sequencing analysis encompassing 2,023,018C>T in BWS-s043. The maternal allele contained a *de novo* variant that was heavily methylated in BWS-s043, while differential methylation was maintained in other family members and normal controls without the variant (Fig. S2a).

Table 1. Variants found in this study[a]

Patient ID	MI of ICR1 (%)	Variant	Position (GRCh37/hg19 chr11)	Location	Transmission	Heterozygosity in normal population
BWS-047	100	G>Gdel	2,024,428	Centromeric outside of ICR1 (5′ of CTS1)	Maternal	2/116 (rs200288360)
		CT>CT del	2,022,561–2,022,562	Between A2 and B4	Maternal	na
BWS-s043	86	G>C	2,022,565	Between A2 and B4	Maternal	0/115
		C>T	2,023,018	A2 (OCT-binding site 1)	*De novo*	0/107
BWS-s061	76	C>T	2,023,497	B5 (5′ of CTS3)	Paternal	2/105
BWS-s081	67	C>T	2,025,777	Centromeric outside of ICR1 (3′ of OCT-binding site 0)	Paternal	0/106
BWS-s100	67	C>A	2,021,145	B1 (3′ of CTS6)	Maternal	0/105
SRS-002	4	G>Gdel	2,024,364	B7 (5′ of CTS1)	Unknown	0/106
SRS-s03	24	C>T	2,021,103	B1 (3′ of CTS6)	Maternal	0/106

ICR, imprinting control region; MI, methylation index; na, not analyzed.
[a]Parents' DNA were not available for SRS-002.

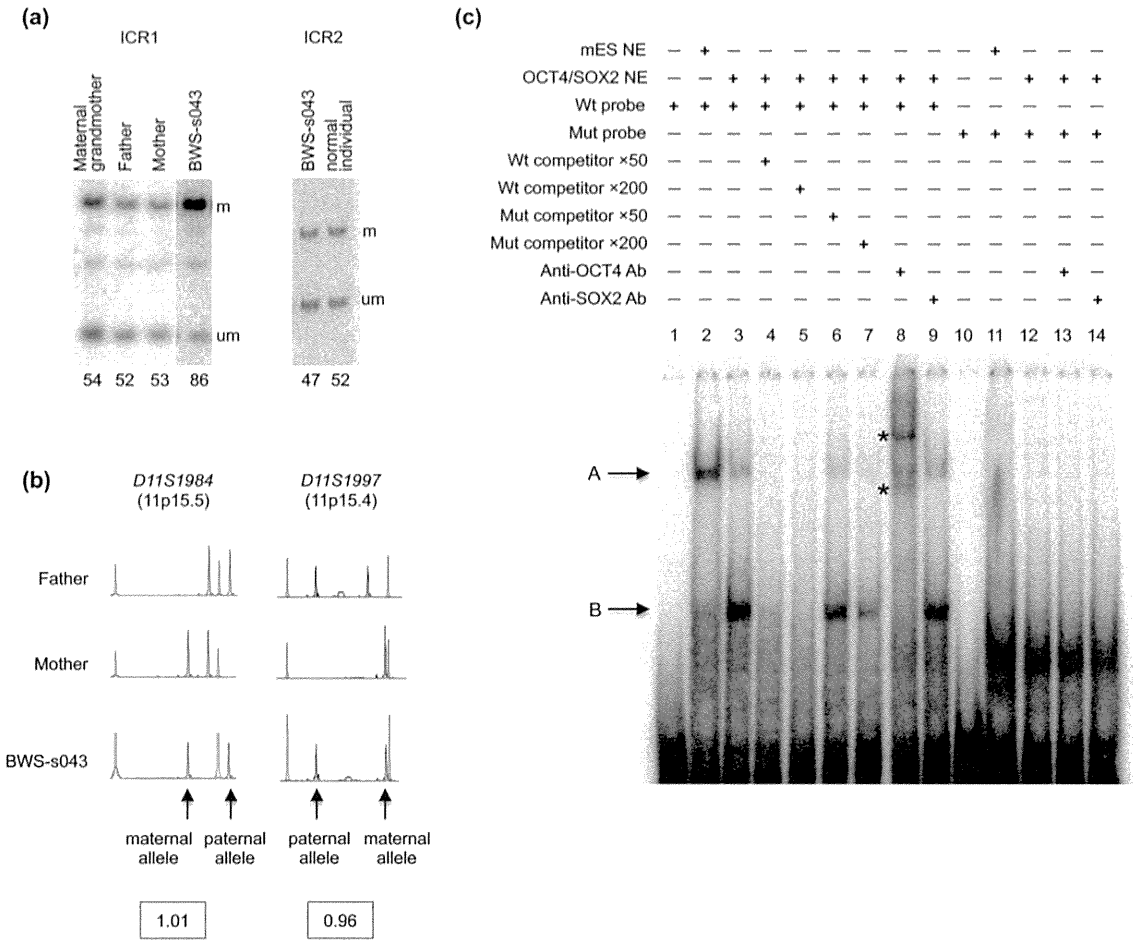

Fig. 2. Methylation-sensitive Southern blots and microsatellite analysis of BWS-s043, and electrophoretic mobility shift assay (EMSA) for 2,023,018C>T. (**a**) Methylation-sensitive Sothern blots of ICR1 and ICR2. Methylation indices [MI, %] are shown below each lane. MI was calculated using the equation $M/(M+U) \times 100$, where M is the intensity of the methylated band and U is the intensity of the unmethylated band. m, methylated band; um, unmethylated band. BWS-s043 showed ICR1-GOM, whereas the relatives did not. Methylation statuses of CTS1 and CTS4 are shown in Fig. S2b,c. Methylation of ICR2 in BWS-s043 was normal. (**b**) Microsatellite analysis at 11p15.4-p15.5. Ratios of the paternal allele to the maternal allele in BWS-s043 were approximately 1, indicating no uniparental disomy. Red peaks are molecular markers. (**c**) EMSA using the wild-type (Wt) probe and the mutant (Mut) probe encompassing 2,023,018C>T. The unlabeled Wt probe or Mut probe (×50 or ×200 molar excess) was used as a competitor. The arrows and asterisks indicate the protein-DNA complexes (A and B) and supershifted complexes, respectively. mES NE, nuclear extract from mouse ES cells; OCT4/SOX2 NE, nuclear extract from human HEK293 cells expressing OCT4/SOX2; Ab, antibody.

for BWS-s043, were not located at any protein-binding sites that have been reported as involved in methylation imprinting (CTCF, OCT, and ZFP57) (3, 4, 10, 12, 16). Furthermore, we did not find any protein-oligonucleotide complexes in EMSA using mouse ES nuclear extracts and oligonucleotide probes encompassing all variants, except for BWS-s043 (Fig. S1). Therefore, we analyzed further three variants in BWS-s043, which were in and around the OCT-binding site 1.

First, we re-confirmed that BWS-s043 showed GOM near CTS6 within ICR1, but it did not demonstrate LOM at ICR2, paternal uniparental disomy of chromosome 11, or a *CDKN1C* mutation (Fig. 2a,b, and data not shown). The 2,023,018C>T variant was located in the second octamer motif of OCT-binding site 1 within repeat A2 (Fig. 1a). The other two variants were located approximately 450 bp on the telomeric side of the 2,023,018C>T variant, between repeats A2 and B4 (Fig. 1a, Table 1). The 2,023,018C>T variant was absent in other family members, indicating a *de novo* variant (Fig. 1a). To clarify if the *de novo* variant in the patient occurred on the maternal or paternal allele, we performed haplotype analysis with PCR covering all three variants. We found all three variants were located on the same allele and the 2,023,018C>T variant occurred *de novo* on the maternal allele because the 2,022,561–562CT>delCT and 2,022,565G>C variants were on the maternal allele in the patient (Fig. 1b,c).

Next, we investigated the methylation status of ICR1. Methylation-sensitive Southern blots and bisulfite sequencing showed normal methylation of ICR1 in the parents and the maternal grandmother (Figs 2a and S2). As for the 2,022,561-562CT>delCT and the 2,022,565G>C variants, the variant allele was unmethylated in the mother, but methylated in the grandmother (Fig. 1d). On the basis of methylation

analysis, the variant allele in the grandmother must have been transmitted by her father, and that in the mother must have been transmitted by her mother. The results indicated that the variant allele could be either methylated or unmethylated during gametogenesis, strongly suggesting no relation between the variants and ICR1-GOM. On the other hand, bisulfite sequencing including the 2,023,018C>T variant revealed that both the variant and wild-type alleles were heavily methylated in the patient (Fig. 1e), while differential methylation was maintained in other family members and normal controls without the variant (Fig. S2a). As the *de novo* variant on the maternal allele was located within the OCT-binding site, which is required for the maintenance of the unmethylated status in a mouse model, the variant was likely involved in ICR1-GOM (17, 18).

Finally, we performed EMSA to determine if 2,023,018C>T influenced the binding ability of nuclear protein factors, such as OCT4 and SOX2 (Fig. 2c). The wild-type probe formed two complexes (A and B) with the nuclear extracts of mouse ES cells and HEK293 cells expressing OCT4/SOX2 (lanes 2 and 3), whereas such complexes were not observed in the mutant probe (lanes 11 and 12). Complexes A and B competed more efficiently with wild-type than with the mutant competitor (lanes 4 to 7). Furthermore, complex B, but not A, was supershifted with the antibody against OCT4 (lane 8). The supershift did not occur with the antibody against SOX2 and with both antibodies using the mutant probe (lanes 9, 13, and 14). These data demonstrated that 2,023,018C>T abrogated binding ability of a nuclear factor, most likely OCT4. Taken together, our data strongly suggest that 2,023,018C>T is a mutation that could prevent OCT4 binding to the OCT-binding site and induce ICR1-GOM, leading to BWS.

Discussion

We identified a novel *de novo* point mutation, chr11: 2,023,018C>T, in OCT-binding site 1 within repeat A2 in a BWS patient with ICR1-GOM. Our data strongly suggest the involvement of the mutation in GOM at ICR1. In a mouse cell model, the evolutionarily well-conserved dyad octamer motif within ICR1, which is bound by OCT protein, has been shown to be required for the maintenance of unmethylated status competing against *de novo* methylation (17). In addition, the importance of a SOX motif flanked by an OCT motif has also been reported (19). Recent studies have shown that the SOX–OCT motif functions to maintain unmethylated status *in vitro* and *in vivo*; a cooperative function of CTCF and OCT/SOX for maintenance of differential methylation has been suggested as responsible (18, 19). Although there is one OCT-binding site in mice, three evolutionarily conserved OCT-binding sites (0, 1, 2) are located in and around ICR1 in humans. As all mutations and the small deletion previously reported in addition to our case occurred in site 1 within repeat A2 (Fig. 1a), site 1 within repeat A2 likely plays a more important role for maintaining unmethylated status of maternal ICR1 in humans than the other OCT-binding sites (10, 12, 13).

ICR1-GOM cases, including ours, with mutations/deletions also show partial hypermethylation in spite of pre-existent genetic aberrations in the oocyte (9, 12, 13, 20), suggesting aberrant hypermethylation at ICR1 would also be stochastically acquired at a cellular level even in the existence of such aberrations.

As for SRS, including familial cases, the ICR1 mutation has not been found except in one sporadic case to date (10). We did not find any promising mutations in this study, suggesting the cause of ICR1 methylation defects to differ between SRS and BWS.

In conclusion, we identified a novel *de novo* point mutation of OCT-binding site 1 within repeat A2, a location suggested to play an important role for maintaining the unmethylated status of maternal ICR1 in humans, on the maternal allele in a BWS patient with ICR1-GOM. However, genetic aberrations of ICR1 explain only 20% of BWS cases with ICR1-GOM (10). As aberrant methylation may occur as a consequence of stochastic events or environmental influences irrespective of ICR1 mutations, unknown causes for ICR1 methylation defects should be clarified.

Supporting Information

The following Supporting information is available for this article:

Fig. S1. EMSA for all variants found in this study, except for those in BWS-047 and BWS-s061, using the nuclear extract from mouse ES cells. The variant in BWS-s081 was located outside of ICR1, and a CpG site within the probe sequence was mostly unmethylated in three normal controls (data not shown). Thus, an unmethylated probe was used for it. Since the variants in BWS-s100 and SRS-s03 were located 3′ of CTS6 and found on the maternal allele, unmethylated probes were used for them. As for the variant in SRS-002, it was located 5′ of CTS1 but its parental origin was unknown. Thus, both unmethylated and methylated probes were used for it. There was no difference between a wt-probe and a variant-probe in each variant except for the BWS-s043 mutation. A wt-probe for the BWS-s043 mutation formed two complexes, whereas such complexes were not observed with a probe for the mutation. These results suggested that only the BWS-s043 mutation affected the protein–DNA interaction (see text and Fig. 2c for details). WT, probe for the wild-type sequence; MUT, probe for the BWS-s043 mutation; VAR, probe for the variant sequence; um, unmethylated probe; me, methylated probe; mES NE, nuclear extract from mouse ES cells.
Fig. S2. Bisulfite sequencing of the region encompassing the 2,023,018 variant, CTS1, and CTS4. (**a**) Results for the 2,023,018 variant. In the healthy members of the BWS-s043 family, comprised of the maternal grandmother, mother, and father, showed differential methylation. Three normal controls also showed differential methylation. In particular, normal control 3 was heterozygous for a SNP (rs61520309) and showed differential methylation in an allele-dependent manner. Open and filled circles indicate unmethylated and methylated CpG sites, respectively. (**b**) Results for CTS1. Two normal controls that were heterozygous for a SNP (rs2525885) showed differential methylation. The healthy family members also showed differential methylation, whereas the patient, BWS-s043, showed aberrant hypermethylation. CpG sites within CTS1 are indicated by a short horizontal line. X indicates T of the SNP (rs2525885). (**c**) Results for CTS4. The healthy family members and two normal controls showed differential

methylation. Among them, the parents and two normal controls were heterozygous for a SNP (rs2525883). The patient, BWS-s043, showed aberrant hypermethylation. CpG sites within CTS4 were indicated by a short horizontal line. X indicates T of the SNP (rs2525883).

Table S1. PCR primers and oligonucleotide probes used in this study.

Additional Supporting information may be found in the online version of this article.

Acknowledgements

This study was supported, in part, by a Grant for Research on Intractable Diseases from the Ministry of Health, Labor, and Welfare; a Grant for Child Health and Development from the National Center for Child Health and Development; a Grant-in-Aid for Challenging Exploratory Research; and, a Grant-in-Aid for Scientific Research (C) from the Japan Society for the Promotion of Science.

References

1. Weksberg R, Shuman C, Beckwith JB. Beckwith–Wiedemann syndrome. Eur J Hum Genet 2010: 18: 8–14.
2. Gicquel C, Rossignol S, Cabrol S et al. Epimutation of the telomeric imprinting center region on chromosome 11p15 in Silver–Russell syndrome. Nat Genet 2005: 37: 1003–1007.
3. Bell AC, Felsenfeld G. Methylation of a CTCF-dependent boundary controls imprinted expression of the Igf2 gene. Nature 2000: 405: 482–485.
4. Hark AT, Schoenherr CJ, Katz DJ, Ingram RS, Levorse JM, Tilghman SM. CTCF mediates methylation-sensitive enhancer-blocking activity at the H19/Igf2 locus. Nature 2000: 405: 486–489.
5. Schoenherr CJ, Levorse JM, Tilghman SM. CTCF maintains differential methylation at the Igf2/H19 locus. Nat Genet 2003: 33: 66–69.
6. Pant V, Mariano P, Kanduri C et al. The nucleotides responsible for the direct physical contact between the chromatin insulator protein CTCF and the H19 imprinting control region manifest parent of origin-specific long-distance insulation and methylation-free domains. Genes Dev 2003: 17: 586–590.
7. Sparago A, Cerrato F, Vernucci M, Ferrero GB, Silengo MC, Riccio A. Microdeletions in the human H19 DMR result in loss of IGF2 imprinting and Beckwith–Wiedemann syndrome. Nat Genet 2004: 36: 958–960.
8. Prawitt D, Enklaar T, Gärtner-Rupprecht B et al. Microdeletion of target sites for insulator protein CTCF in a chromosome 11p15 imprinting center in Beckwith–Wiedemann syndrome and Wilms' tumor. Proc Natl Acad Sci U S A 2005: 102: 4085–4090.
9. Beygo J, Citro V, Sparago A et al. The molecular function and clinical phenotype of partial deletions of the IGF2/H19 imprinting control region depends on the spatial arrangement of the remaining CTCF-binding sites. Hum Mol Genet 2013: 22: 544–557.
10. Demars J, Shmela ME, Rossignol S et al. Analysis of the IGF2/H19 imprinting control region uncovers new genetic defects, including mutations of OCT-binding sequences, in patients with 11p15 fetal growth disorders. Hum Mol Genet 2010: 19: 803–814.
11. Quenneville S, Verde G, Corsinotti A et al. In embryonic stem cells, ZFP57/KAP1 recognize a methylated hexanucleotide to affect chromatin and DNA methylation of imprinting control regions. Mol Cell 2011: 44: 361–372.
12. Poole RL, Docherty LE, Al Sayegh A et al. Targeted methylation testing of a patient cohort broadens the epigenetic and clinical description of imprinting disorders. Am J Med Genet A 2013: 161: 2174–2182.
13. Berland S, Appelbäck M, Bruland O et al. Evidence for anticipation in Beckwith–Wiedemann syndrome. Eur J Hum Genet 2013: 21: 1344–1348.
14. Higashimoto K, Nakabayashi K, Yatsuki H et al. Aberrant methylation of H19-DMR acquired after implantation was dissimilar in soma versus placenta of patients with Beckwith–Wiedemann syndrome. Am J Med Genet A 2012: 158A: 1670–1675.
15. Soejima H, Nakagawachi T, Zhao W et al. Silencing of imprinted CDKN1C gene expression is associated with loss of CpG and histone H3 lysine 9 methylation at DMR-LIT1 in esophageal cancer. Oncogene 2004: 23: 4380–4388.
16. Mackay DJ, Callaway JL, Marks SM et al. Hypomethylation of multiple imprinted loci in individuals with transient neonatal diabetes is associated with mutations in ZFP57. Nat Genet 2008: 40: 949–951.
17. Hori N, Nakano H, Takeuchi T et al. A dyad Oct-binding sequence functions as a maintenance sequence for the unmethylated state within the H19/Igf2-imprinted control region. J Biol Chem 2002: 277: 27960–27967.
18. Sakaguchi R, Okamura E, Matsuzaki H, Fukamizu A, Tanimoto K. Sox-Oct motifs contribute to maintenance of the unmethylated H19 ICR in YAC transgenic mice. Hum Mol Genet 2013: 22: 4627–4637.
19. Hori N, Yamane M, Kouno K, Sato K. Induction of DNA demethylation depending on two sets of Sox2 and adjacent Oct3/4 binding sites (Sox-Oct motifs) within the mouse H19/insulin-like growth factor 2 (Igf2) imprinted control region. J Biol Chem 2012: 287: 44006–44016.
20. Sparago A, Russo S, Cerrato F et al. Mechanisms causing imprinting defects in familial Beckwith–Wiedemann syndrome with Wilms' tumour. Hum Mol Genet 2007: 16: 254–264.

ORIGINAL RESEARCH ARTICLE | Genetics inMedicine

Open

Comprehensive and quantitative multilocus methylation analysis reveals the susceptibility of specific imprinted differentially methylated regions to aberrant methylation in Beckwith–Wiedemann syndrome with epimutations

Toshiyuki Maeda, MD[1,2], Ken Higashimoto, PhD[1], Kosuke Jozaki, PhD[1], Hitomi Yatsuki, PhD[1], Kazuhiko Nakabayashi, PhD[3], Yoshio Makita, PhD[4], Hidefumi Tonoki, PhD[5], Nobuhiko Okamoto, MD[6], Fumio Takada, PhD[7], Hirofumi Ohashi, PhD[8], Makoto Migita, PhD[9], Rika Kosaki, MD[10], Keiko Matsubara, PhD[11], Tsutomu Ogata, PhD[12], Muneaki Matsuo, PhD[2], Yuhei Hamasaki, PhD[2], Yasufumi Ohtsuka, MD[1,2], Kenichi Nishioka, PhD[1], Keiichiro Joh, PhD[1], Tsunehiro Mukai, PhD[13], Kenichiro Hata, PhD[3] and Hidenobu Soejima, PhD[1]

Purpose: Expression of imprinted genes is regulated by DNA methylation of differentially methylated regions (DMRs). Beckwith–Wiedemann syndrome is an imprinting disorder caused by epimutations of DMRs at 11p15.5. To date, multiple methylation defects have been reported in Beckwith–Wiedemann syndrome patients with epimutations; however, limited numbers of DMRs have been analyzed. The susceptibility of DMRs to aberrant methylation, alteration of gene expression due to aberrant methylation, and causative factors for multiple methylation defects remain undetermined.

Methods: Comprehensive methylation analysis with two quantitative methods, matrix-assisted laser desorption/ionization mass spectrometry and bisulfite pyrosequencing, was conducted across 29 DMRs in 54 Beckwith–Wiedemann syndrome patients with epimutations. Allelic expressions of three genes with aberrant methylation were analyzed. All DMRs with aberrant methylation were sequenced.

Results: Thirty-four percent of *KvDMR1*–loss of methylation patients and 30% of *H19*DMR–gain of methylation patients showed multiple methylation defects. Maternally methylated DMRs were susceptible to aberrant hypomethylation in *KvDMR1*–loss of methylation patients. Biallelic expression of the genes was associated with aberrant methylation. *Cis*-acting pathological variations were not found in any aberrantly methylated DMR.

Conclusion: Maternally methylated DMRs may be vulnerable to DNA demethylation during the preimplantation stage, when hypomethylation of *KvDMR1* occurs, and aberrant methylation of DMRs affects imprinted gene expression. *Cis*-acting variations of the DMRs are not involved in the multiple methylation defects.

Genet Med advance online publication 8 May 2014

Key Words: Beckwith–Wiedemann syndrome; DNA methylation; differentially methylated region; genomic imprinting; multiple methylation defects

INTRODUCTION

Genomic imprinting is an epigenetic phenomenon that leads to parent-specific differential expression of a subset of mammalian genes. Most imprinted genes are clustered in regions called imprinting domains, and the expression of imprinted genes within these domains is regulated by imprinting control regions.[1,2] Differentially methylated regions (DMRs), which are defined as having DNA methylation on only one of the two parental alleles, play critical roles in the regulation of imprinting. There are two kinds of DMRs: maternally methylated DMRs (matDMRs) and paternally methylated DMRs (patDMRs). In addition, there is another classification, gametic DMRs and somatic DMRs, based on the timing of the establishment of differential methylation. Gametic DMRs acquire DNA methylation during gametogenesis, and the methylation is maintained from zygote to somatic cells during all developmental stages. Most gametic DMRs are identical to imprinting control regions. On the other hand, somatic DMRs are established during early embryogenesis after fertilization under the control of nearby imprinting control regions.[1,2] Because imprinted genes play an important role in the growth and development of embryos, placental formation, and metabolism, aberrant expression of

[1]Division of Molecular Genetics and Epigenetics, Department of Biomolecular Sciences, Faculty of Medicine, Saga University, Saga, Japan; [2]Department of Pediatrics, Faculty of Medicine, Saga University, Saga, Japan; [3]Department of Maternal–Fetal Biology, National Research Institute for Child Health and Development, Tokyo, Japan; [4]Education Center, Asahikawa Medical University, Asahikawa, Japan; [5]Department of Pediatrics, Maternal, Perinatal, and Child Medical Center, Tenshi Hospital, Sapporo, Japan; [6]Department of Medical Genetics, Osaka Medical Center and Research Institute for Maternal and Child Health, Izumi, Japan; [7]Department of Medical Genetics, Kitasato University Graduate School of Medical Sciences, Kanagawa, Japan; [8]Division of Medical Genetics, Saitama Children's Medical Center, Saitama, Japan; [9]Department of Pediatrics, Nippon Medical School, Tokyo, Japan; [10]Division of Medical Genetics, National Center for Child Health and Development, Tokyo, Japan; [11]Department of Molecular Endocrinology, National Research Institute for Child Health and Development, Tokyo, Japan; [12]Department of Pediatrics, Hamamatsu University School of Medicine, Hamamatsu, Japan; [13]Nishikyushu University, Saga, Japan. Correspondence: Hidenobu Soejima (soejimah@cc.saga-u.ac.jp)

Submitted 10 November 2013; accepted 7 April 2014; advance online publication 8 May 2014. doi:10.1038/gim.2014.46

imprinted genes due to epigenetic or genetic abnormalities is implicated in the pathogenesis of some human disorders, such as congenital anomalies and tumors.[1,2]

Beckwith–Wiedemann syndrome (BWS; Online Mendelian Inheritance in Man (OMIM) #130650) is an imprinting disease that is characterized by prenatal and postnatal macrosomia, macroglossia, abdominal wall defects, and variable minor features. The relevant imprinted chromosomal region in BWS is 11p15.5, which consists of two imprinted domains, *IGF2/H19* and *CDKN1C/KCNQ1OT1*, *H19*DMR and *Kv*DMR1 being the respective imprinting control regions.[3–5] Among several causative alterations identified so far, loss of methylation (LOM) at *Kv*DMR1 and gain of methylation (GOM) at *H19*DMR are isolated epimutations. Hypomethylation at multiple imprinted DMRs has been reported in patients with transient neonatal diabetes mellitus type 1,[6] and the same phenomenon, referred to as multiple methylation defects (MMDs), has been reported in BWS patients with *Kv*DMR1-LOM.[7–13] However, although the human genome contains more than 30 imprinting domains (http://www.geneimprint.com), a limited number of imprinted DMRs have been analyzed so far, with the exception of a report by Court et al.[12] In addition, methods used for methylation analysis have ranged from nonquantitative to quantitative approaches, and although some studies have used only one method for methylation analysis,[8,9,11] others have used two or more in conjuction.[7,10–13] Furthermore, the questions of whether susceptibility to aberrant methylation is different in each type of DMR, whether aberrant methylation indeed affects imprinted gene expression, and what causative factors are responsible for MMDs still remain unanswered. To clarify these issues, we have conducted a comprehensive methylation screening in BWS patients with *Kv*DMR1-LOM or *H19*DMR-GOM with a quantitative method, matrix-assisted laser desorption/ionization mass spectrometry (MALDI-TOF MS), on 29 imprinted DMRs, which represents the largest number of DMRs analyzed to date, followed by confirmation with another quantitative method, bisulfite pyrosequencing. We also performed gene expression analysis and sequencing of aberrantly methylated DMRs. We found that matDMRs are susceptible to aberrant methylation. We also found alterations in imprinted gene expression due to the aberrant methylation and no *cis*-acting pathological variations in DMRs with MMDs.

MATERIALS AND METHODS

Patients

Fifty-four BWS patients (25 boys, 26 girls, 3 gender-unspecified patients; average age: 3.0 years (0–13.9 years)) and their parents were enrolled in this study. Among them, 46 patients met clinical criteria for BWS as described by Weksberg et al.[3] and 6 patients met clinical criteria as described by DeBaun et al.[14] (**Supplementary Table S1** online). Because two patients were clinically diagnosed more than 20 years ago, their specific diagnostic criteria were unknown. The methylation statuses of *H19*DMR and *Kv*DMR1, paternal uniparental disomy of chromosome 11 (upd(11)pat), and *CDKN1C* mutations were screened as described previously.[15–17] Peripheral blood samples of most patients were subjected to standard G-banding chromosome analysis and/or high-resolution G-band patterning of human chromosome 11, but neither assay showed any abnormalities in any patient (data not shown). Among the 54 patients, 44 displayed *Kv*DMR1-LOM but did not show other causative alterations, including *H19*DMR-GOM, upd(11)pat, and *CDKN1C* mutations (data not shown). The remaining 10 patients displayed *H19*DMR-GOM but did not show other causative alterations (data not shown). We sequenced the entire *H19*DMR in *H19*DMR-GOM patients and found no mutations.[18] We used the peripheral blood samples of 24 children (11 boys, 13 girls; average age: 3.8 years (range of 0–8 years)) who visited the Department of Pediatrics, Saga University Hospital, as normal controls having only mild illness such as common cold. This study was approved by the Ethics Committee for Human Genome and Gene Analyses of the Faculty of Medicine, Saga University. Written informed consent was obtained from the parents or the guardians of the patients and participants.

DNA isolation and bisulfite conversion

Genomic DNA was extracted from the peripheral blood of patients using the FlexiGene DNA Kit (Qiagen, Hilden, Germany) according to the manufacturer's instructions. A total of 1 μg of genomic DNA was subjected to bisulfite conversion using the EZ DNA Methylation Kit (Zymo Research, Irvine, CA), and then the converted DNA was eluted in 100 μl of water. Unmethylated control DNA was created by whole-genome amplification using the REPLI-g Mini Kit (Qiagen). To prepare fully methylated control DNA, the unmethylated DNA created by whole-genome amplification was treated twice with *Sss*I methylase.

Methylation analysis by MALDI-TOF MS

The DNA methylation status of imprinted DMRs was analyzed by MALDI-TOF MS analysis with a MassARRAY system (Sequenom, San Diego, CA) as previously described.[19,20] Briefly, each DMR was amplified by bisulfite-mediated polymerase chain reaction (PCR) using a primer set containing a primer carrying the T7 promoter sequence at the 5′ end. In vitro transcription of the PCR product was performed with T7 RNA polymerase, and the transcript was subjected to uracil-specific cleavage with RNase A. MALDI-TOF MS analysis of the cleaved fragments produced signal pattern pairs indicative of nonmethylated and methylated DNA. Epityper software (Sequenom) analysis of the signals yielded a methylation index (MI) ranging from 0 (no methylation) to 1 (full methylation) for each CpG unit, which contained one or more CpG sites. Aberrant methylation of a CpG unit was defined as the condition in which the difference of MIs between each patient and the average of normal controls exceeded 0.15. This definition was based on our finding in methylation-sensitive Southern blots, which revealed that the differences in MI for *Kv*DMR1-LOM or *H19*DMR-GOM in BWS patients were ≥0.15 (data not shown). Because the analyzed DMRs included several CpG units, aberrant methylation of each DMR was defined as the situation in which more

than 60% of the total number of analyzed CpG units showed aberrant methylation (with the MI difference exceeding 0.15). In the case of *IGF2*-DMR0, the three CpG sites were analyzed based on previous reports.[21,22] All primers used in this study are shown in **Supplementary Table S2** online.

Methylation analysis by bisulfite pyrosequencing

The aberrant methylation status of DMRs identified by MALDI-TOF MS was confirmed by bisulfite pyrosequencing using QIAGEN PyroMark Q24 according to the manufacturer's instructions (Qiagen). Primers for bisulfite-mediated PCR and pyrosequencing were designed using PyroMark Assay Design 2.0 (Qiagen). In analogy with MALDI-TOF MS analysis, aberrant methylation of a CpG site was defined as the situation in which the difference of MIs between each patient and the average of normal controls exceeded 0.15. Aberrant methylation of each DMR was defined as the condition in which more than 60% of the total number of analyzed CpG sites showed aberrant methylation (with the MI difference exceeding 0.15).

Bisulfite sequencing

Bisulfite sequencing was performed to analyze allelic methylation of *ZDBF2*-DMR. After PCR amplification, the PCR products were cloned into a pT7Blue T-Vector (Novagen, Darmstadt, Germany), and individual clones were sequenced. Parental alleles were distinguished by a single-nucleotide polymorphism (SNP, *rs1861437*) within the DMR.

Expression analysis of *ZDBF2*, *FAM50B*, and *GNAS1A*

Total RNA was extracted from the peripheral blood of patients using the QIAamp RNA Blood Mini Kit (Qiagen). The RNA was treated with RNase-free DNase I, and reverse transcription was performed with random primers. We used SNPs for allelic expression to distinguish between the two parental alleles: *rs10932150* in exon 5 of *ZDBF2*; *rs6597007* in exon 2 of *FAM50B*; and *rs143800311*, which is a 5-bp deletion/insertion variation in exon 1A of *GNAS1A*. Reverse transcription–PCR (RT-PCR) products encompassing the SNPs of *ZDBF2* and *FAM50B* were directly sequenced. The products encompassing the deletion/insertion variation of *GNAS1A* were separated by electrophoresis on an Applied Biosystems 3130 genetic analyzer (Applied Biosystems, Foster City, CA) and then analyzed with GeneMapper software (Applied Biosystems). Total expression levels of *ZDBF2* and *FAM50B* were quantitated by real-time PCR with TaqMan probes (Applied Biosystems). The expression level of each gene was normalized against that of the housekeeping genes encoding hydroxymethylbilane synthase (*HMBS*) and glyceraldehyde-3-phosphate dehydrogenase (*GAPDH*). All quantitative RT-PCRs were performed in triplicate.

Sequencing of aberrantly methylated DMRs

Direct sequencing of all DMRs showing aberrant methylation in *Kv*DMR1-LOM patients was performed to determine whether there was any pathological variation.

Statistical analyses

Fisher's exact test was used for the comparison of aberrant methylated DMRs. Fisher's exact test or Mann–Whitney *U*-test was used for statistical analyses of clinical features between MMDs and monolocus methylation defects in *Kv*DMR1-LOM patients. A P value < 0.05 was considered statistically significant.

RESULTS

Validation of methylation analyses, MALDI-TOF MS, and bisulfite pyrosequencing

First, we selected 37 regions reported previously as imprinted DMRs in the human genome[16,20,23] (refer to http://www.geneimprint.com/). To validate the quantitative capability of MALDI-TOF MS methylation analysis, mixtures of the unmethylated control DNA and the fully methylated control DNA (0, 25, 50, 75, and 100% methylated DNA) were subjected to bisulfite conversion and analyzed. We found a significant correlation between the measured MIs and predicted MIs in all DMRs, except for *GRB10*, *PEG13*, and IG-DMR-CG4 (**Supplementary Figure S1** online). Furthermore, in normal leukocytes, two regions (*TCEB3C*, *USP29*) showed mostly full methylation and three regions (*TP73*, *SPTBN1*, *WT1-AS*) showed mostly no methylation, suggesting that these regions were not differentially methylated in leukocytes (data not shown). Therefore, we excluded these eight regions and decided to analyze the remaining 29 DMRs by MALDI-TOF MS. Second, we obtained MIs from 24 normal controls using MALDI-TOF MS and calculated the average and SD of each CpG unit. We excluded CpG units in which SDs were >0.1 from further analysis. Averages and SDs of all CpG units analyzed in this study are shown in **Supplementary Table S3** online. After the MALDI-TOF MS analysis, we used bisulfite pyrosequencing to confirm the aberrant methylation uncovered. We also obtained MIs from the 24 controls using bisulfite pyrosequencing and calculated the average and SD of each CpG site. We excluded one CpG site in *H19*DMR because its SD was >0.1 due to a known SNP (*rs10732516*). Averages and SDs of control CpG sites are shown in **Supplementary Table S3** online. Finally, we compared the MIs of MALDI-TOF MS and bisulfite pyrosequencing of each DMR and found a significant correlation (**Supplementary Figure S2** online).

Multilocus methylation defects in BWS patients with epimutations

Among the 44 *Kv*DMR1-LOM patients, 15 (34.1%) showed aberrantly methylated DMRs outside of *Kv*DMR1: six showed aberrant methylation at only one DMR, and the other nine showed two or more methylated DMRs (**Figure 1a** and **Supplementary Figure S3** online). The greatest number of aberrantly methylated DMRs was found in patient BWS-s113, who exhibited 12 DMRs. Most of the aberrantly methylated DMRs demonstrated LOM, which was seen at *ARHI*-CG1, *ARHI*-CG2, *ARHI*-CG3, *FAM50B*, *ZAC*, *IGF2R*-DMR2, *MEST*, *NNAT*, *L3MBTL1*, *NESPAS*, *GNASXL*, and *GNAS1A*. Among them, the most frequently hypomethylated DMRs were

ARHI-CG1 and *ARHI*-CG3, found in nine (20.5%) and eight (18.2%) patients, respectively. By contrast, three DMRs, located at *ZDBF2*, *NESP*, and *MCTS2*, showed GOM, which was found in six (13.6%), two (4.5%), and one (2.3%) patients, respectively. *GNASXL*-DMR showed GOM in one patient (2.3%), whereas four patients (9.1%) showed LOM. The other 13 DMRs were not aberrantly methylated in any *Kv*DMR1-LOM patient.

Among the 10 *H19*DMR-GOM patients, all patients showed GOM at the *H19* promoter DMR, which was usually observed with loss of imprinting of *IGF2* (Figure 1b).[24] Four patients showed GOM at either *IGF2*-DMR0 or *IGF2*-DMR2; two patients showed GOM at both. Moreover, both LOM and GOM at other DMRs were found: LOM was found at *INPP5Fv2*-DMR in patients BWS-s015 and BWS-s064, and GOM was found at *NESP*-DMR in patient BWS-s012.

In addition, to exclude aberrantly methylated DMRs resulting from chromosome abnormalities such as uniparental disomy and copy number abnormality, microsatellite analyses using patients' and their parents' DNA were performed on all DMRs showing aberrant methylation. For quantitative analyses, tetranucleotide repeat markers near the imprinted DMRs were used (**Supplementary Materials and Methods** online). We found that no DMRs, except for six DMRs in three patients, exhibited any chromosome abnormalities (summarized in **Supplementary Figure S4** online). These results strongly suggest that the aberrant methylation of DMRs observed was

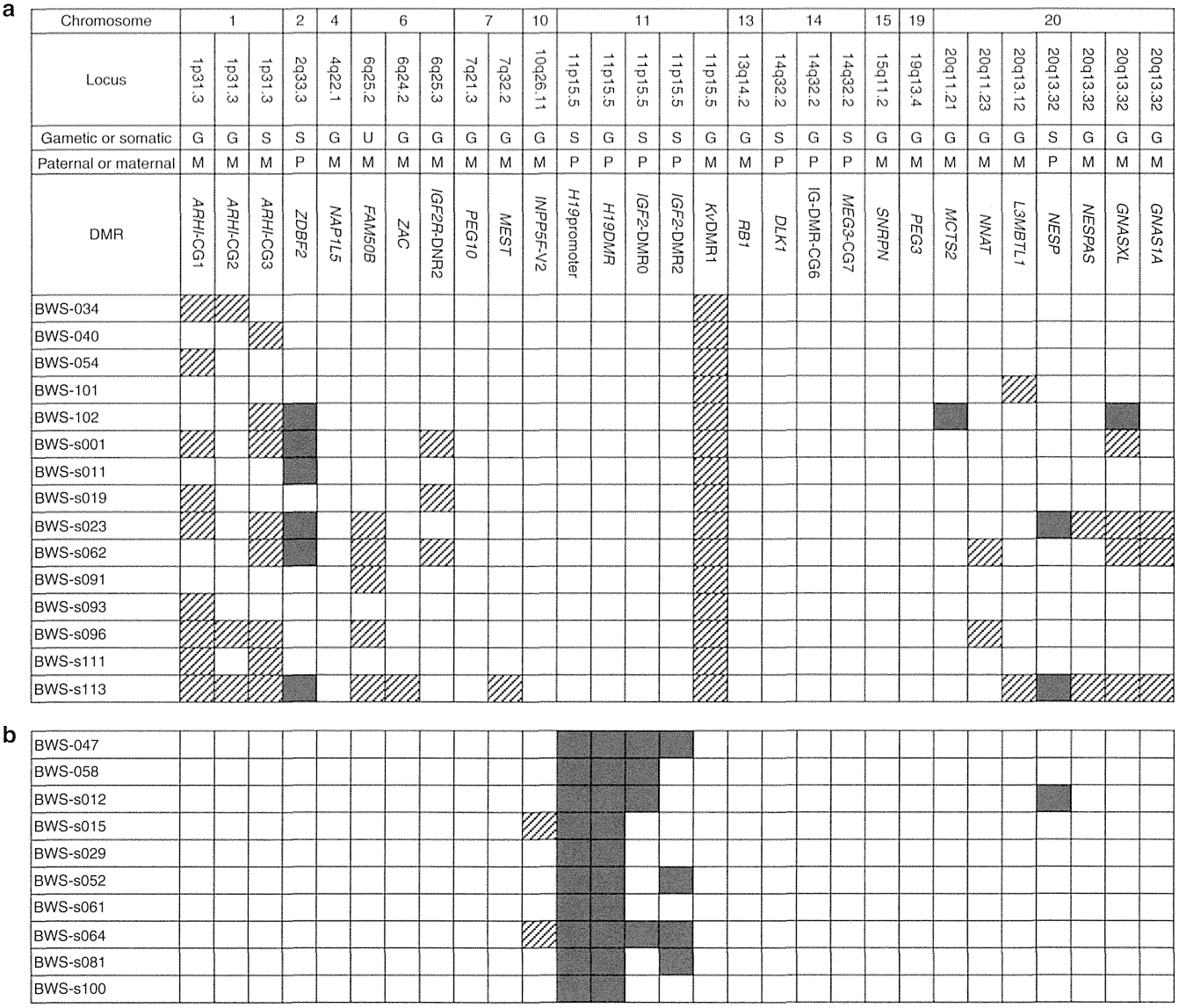

Figure 1 Results of methylation analyses of 29 imprinted differentially methylated regions (DMRs) in Beckwith–Wiedemann syndrome patients with epimutations. (**a**) Results of patients with *Kv*DMR1-LOM. Only the results of multiple methylation defects are shown. Aberrant methylation was confirmed by two quantitative methods: matrix-assisted laser desorption/ionization mass spectrometry and bisulfite pyrosequencing. The definition of aberrant methylation used here is described in the Materials and Methods section. Shaded rectangle: aberrant hypomethylation; dark gray rectangle: aberrant hypermethylation. (**b**) Results of all patients with *H19*DMR-GOM. GOM, gain of methylation; LOM, loss of methylation.

an isolated epimutation and was not due to chromosome abnormalities.

Comparison of aberrantly methylated DMRs

We found that 34.1% (15 of 44) of *Kv*DMR1-LOM patients and 30.0% (3 of 10) of *H19*DMR-GOM patients showed MMDs (**Figure 1a**). There was no statistical difference between them ($P > 0.99$, Fisher's exact test).

Among the 29 DMRs analyzed, there were 20 gametic DMRs and 8 somatic DMRs (**Figure 1a**). The timing of methylation establishment of one DMR (*FAM50B*-DMR) has not yet been determined. On the other hand, there were 20 matDMRs and 9 patDMRs. We investigated whether susceptibility to aberrant methylation differed for each type of DMR in *Kv*DMR1-LOM patients. *Kv*DMR1 itself, a gametic and matDMR, was excluded from this analysis. Several DMRs were mapped to certain imprinted domains, e.g., three DMRs in the *ARHI* domain and four in the *GNAS* domain. However, these DMRs differed by type, and aberrant methylations of these DMRs were not always linked. We also had previously found that DMRs in the *GNAS* domain were independently aberrantly methylated in hepatoblastoma.[20] Therefore, we decided to perform statistical analyses assuming the independence of each DMR.

We first compared gametic DMRs with somatic DMRs and found no significant difference in susceptibility ($P = 0.42$, Fisher's exact test; **Figure 2a**). *FAM50B*-DMR was excluded from this comparison. By contrast, matDMRs were aberrantly methylated more frequently than patDMRs ($P = 0.042$, Fisher's exact test; **Figure 2b**). In addition, among the aberrantly methylated DMRs, 12 showed LOM and 4 showed GOM. When we compared LOM with GOM, LOM preferentially occurred on matDMRs ($P = 0.050$, Fisher's exact test; **Figure 2c**). In this subanalysis, *GNASXL*-DMR was counted as having both GOM and LOM (**Figure 1a**). Furthermore, among the 12 DMRs with LOM, most of them (10) were gametic DMRs. These results suggest that matDMRs are susceptible to aberrant methylation and that gametic maternally methylated DMRs tend to be susceptible to LOM in *Kv*DMR1-LOM patients.

Biallelic expression of imprinted genes induced by aberrant methylation at their corresponding DMRs

We continued our investigation by determining whether allelic expression was associated with the methylation status of the corresponding DMR. We selected three genes (*ZDBF2*, *FAM50B*, and *GNAS1A*) expressed in lymphocytes.[25–27] In the case of *ZDBF2*, bisulfite sequencing of *ZDBF2*-DMR showed paternal monoallelic methylation in normal controls heterozygous for a specific SNP (*rs1861437*), whereas four BWS patients with GOM showed biallelic methylation: these findings were consistent with the results of MALDI-TOF MS and bisulfite pyrosequencing (**Figure 3a,b** and **Supplementary Figure S5** online). Because paternal expression of the *ZDBF2* gene is coupled with methylation of *ZDBF2*-DMR on the paternal allele,[25] biallelic expression due to biallelic methylation was expected. Indeed, three BWS patients heterozygous for a coding SNP (*rs10932150*) with hypermethylated DMRs clearly showed biallelic expression, in contrast with the paternal monoallelic expression in patients with normally methylated DMRs (**Figure 3c**). *FAM50B* and *GNAS1A* were paternally expressed and were coupled with maternal methylation of corresponding DMRs. RT-PCR using coding SNPs (*rs6597007* for *FAM50B* and *rs143800311* for *GNAS1A*) revealed that both genes were expressed biallelically with LOM of each corresponding DMR, which was in contrast with monoallelic expression in the patients with normally methylated DMRs (**Figure 4** and **Supplementary Figure S5** online). It is intriguing that *FAM50B* in patient BWS-s096 and *GNAS1A* in patient BWS-s062 were expressed from the maternal allele despite low-grade LOM,

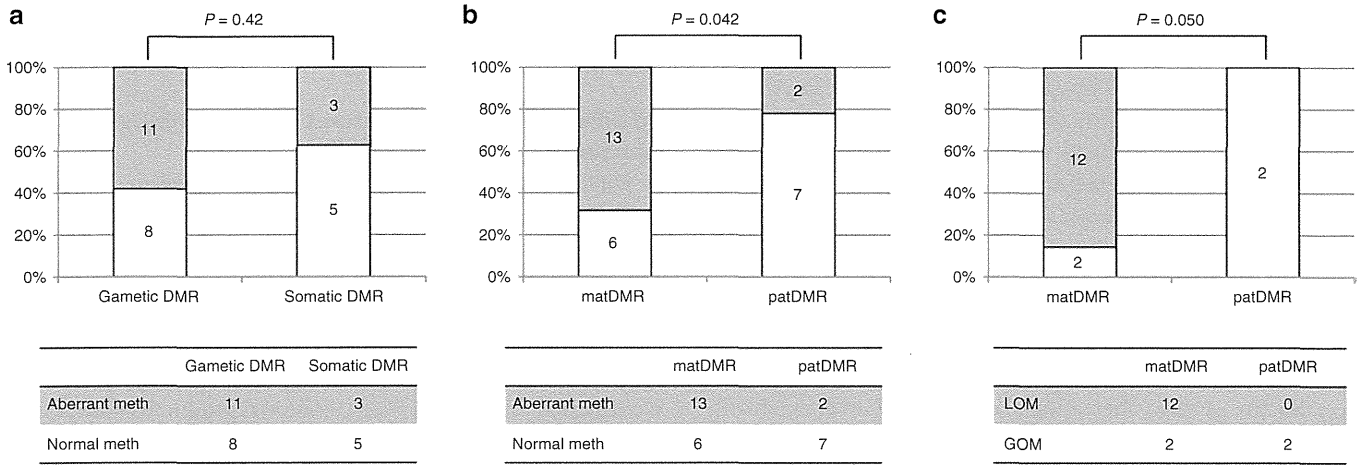

	Gametic DMR	Somatic DMR
Aberrant meth	11	3
Normal meth	8	5

	matDMR	patDMR
Aberrant meth	13	2
Normal meth	6	7

	matDMR	patDMR
LOM	12	0
GOM	2	2

Figure 2 Statistical analyses of aberrantly methylated differentially methylated region (DMRs). (**a**) Comparison of the number of aberrantly methylated DMRs between gametic DMRs and somatic DMRs in *Kv*DMR1-LOM patients. There was no statistical difference between the two DMRs ($P = 0.42$, Fisher's exact test). (**b**) Comparison of the number of aberrantly methylated DMRs between matDMRs and patDMRs in *Kv*DMR1-LOM patients. matDMRs were aberrantly methylated more frequently than patDMRs ($P = 0.042$, Fisher's exact test). (**c**) Comparison of the number of LOMs and GOMs between matDMRs and patDMRs among the aberrantly methylated DMRs in *Kv*DMR1-LOM patients. LOM preferentially occurred on matDMRs ($P = 0.050$, Fisher's exact test). GOM, gain of methylation; LOM, loss of methylation; matDMR, maternally methylated DMR; patDMR, paternally methylated DMR.

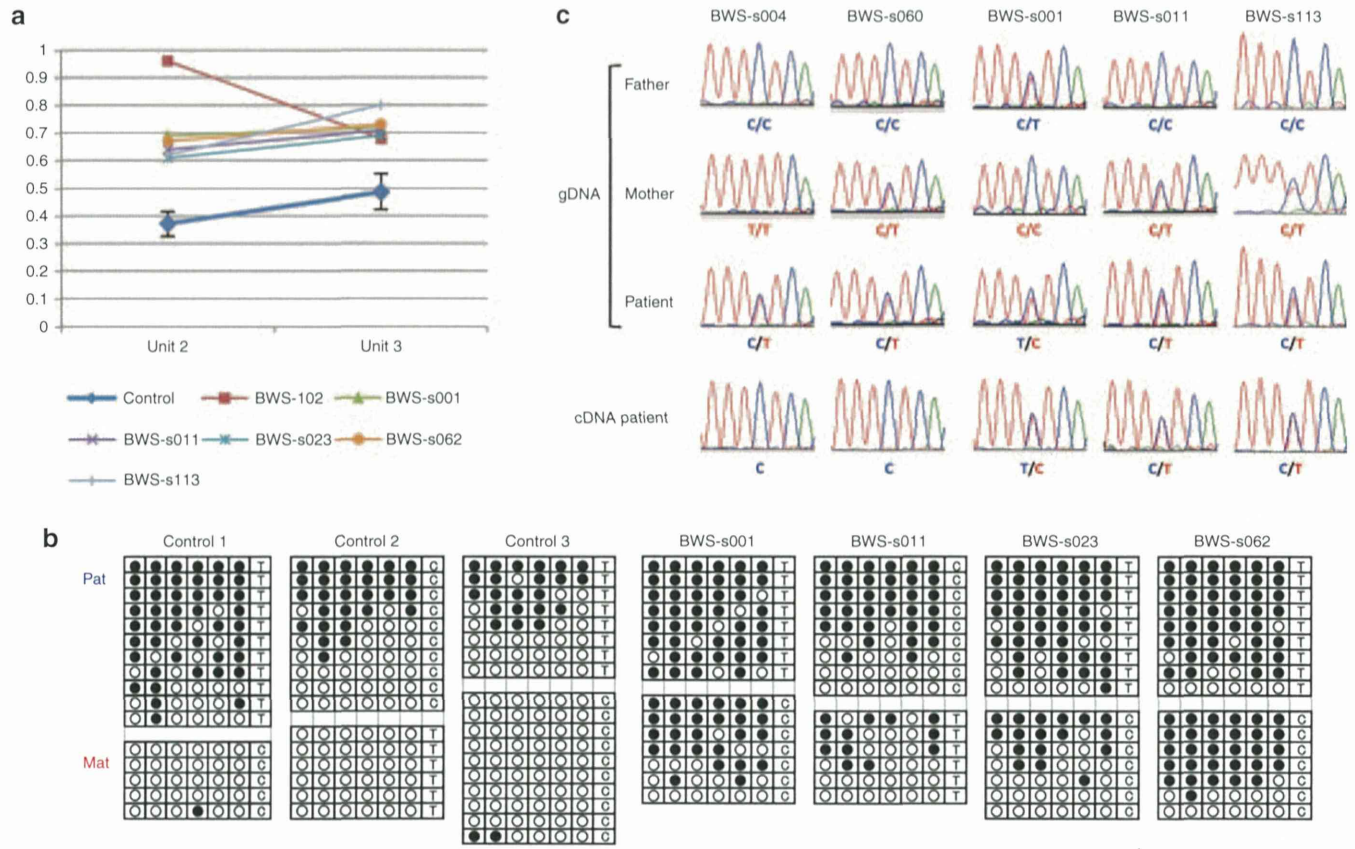

Figure 3 Methylation analysis of *ZDBF2*-DMR and expression analysis of the *ZDBF2* gene. (**a**) Results of matrix-assisted laser desorption/ionization mass spectrometry analysis. Averages with SD of 24 normal controls are shown in blue. Methylation indexes of the patients showing GOM are indicated in different colors. Units 1 and 2 included two and one CpG sites, respectively. (**b**) Results of bisulfite sequencing. Normal controls show monoallelic differential methylation, whereas four Beckwith–Wiedemann syndrome (BWS) patients (BWS-s001, BWS-s011, BWS-s023, and BWS-s060) show biallelic methylation. Two parental alleles were distinguished by a SNP (*rs1861437*). Mat, maternal allele; Pat, paternal allele. (**c**) Results of expression analysis of the *ZDBF2* gene. Three BWS patients (BWS-s001, BWS-s011, and BWS-s113) heterozygous for a coding SNP (*rs10932150*) with GOM clearly showed biallelic expression; by contrast, two patients with normally methylated differentially methylated region (DMRs) exhibited paternal monoallelic expression (patients BWS-s004 and BWS-s060). gDNA, genomic DNA; GOM, gain of methylation; SNP, single-nucleotide polymorphism.

which suggests that our definition of aberrant methylation is appropriate. In addition, we investigated the expression levels of *ZDBF2* and *FAM50B* by quantitative RT-PCR. The expression levels in patients with aberrantly methylated DMRs were higher than those in patients with normally methylated DMRs (**Supplementary Figure S6** online). These results indicate that allelic expression and expression levels were indeed associated with the methylation status of the corresponding DMR in patients with MMDs.

Lack of pathological variation in all aberrantly methylated DMRs in *Kv*DMR1-LOM patients

Because the genetic aberrations of *H19*DMR explained only ~20% of BWS patients with *H19*DMR-GOM,[28] we hypothesized the existence of *cis*-acting variations within aberrantly methylated DMRs. Therefore, we sequenced all aberrantly methylated DMRs, including *Kv*DMR1, in *Kv*DMR1-LOM patients. However, no variations were found in any aberrantly hypomethylated DMRs, except for four known SNPs (summarized in **Supplementary Figure S7** online), suggesting that *cis*-acting pathological variations are not involved in aberrant methylation of these DMRs.

No difference in clinical features between MMDs and monolocus methylation defects

In *Kv*DMR1-LOM patients, there was no significant difference in clinical features between MMDs and monolocus methylation defects, which demonstrated LOM only at *Kv*DMR1 (**Table 1**). Among 27 patients with *Kv*DMR1-LOM for whom information on conception was available, one patient was conceived using intracytoplasmic sperm injection, two were from artificial insemination by the husband, and two were from ovulation stimulation. We searched for a link between assisted reproductive technology and MMD but could find no relationship (**Table 1**). The average age of neither the mother nor the father differed between patients with MMDs versus those with monolocus methylation defects (**Table 1**). The fact that monozygotic twins discordant for BWS were found predominantly for females suggests an insufficient amount of DNA methyltransferase 1 (DNMT1) to maintain *Kv*DMR1 methylation during the overlap in timing

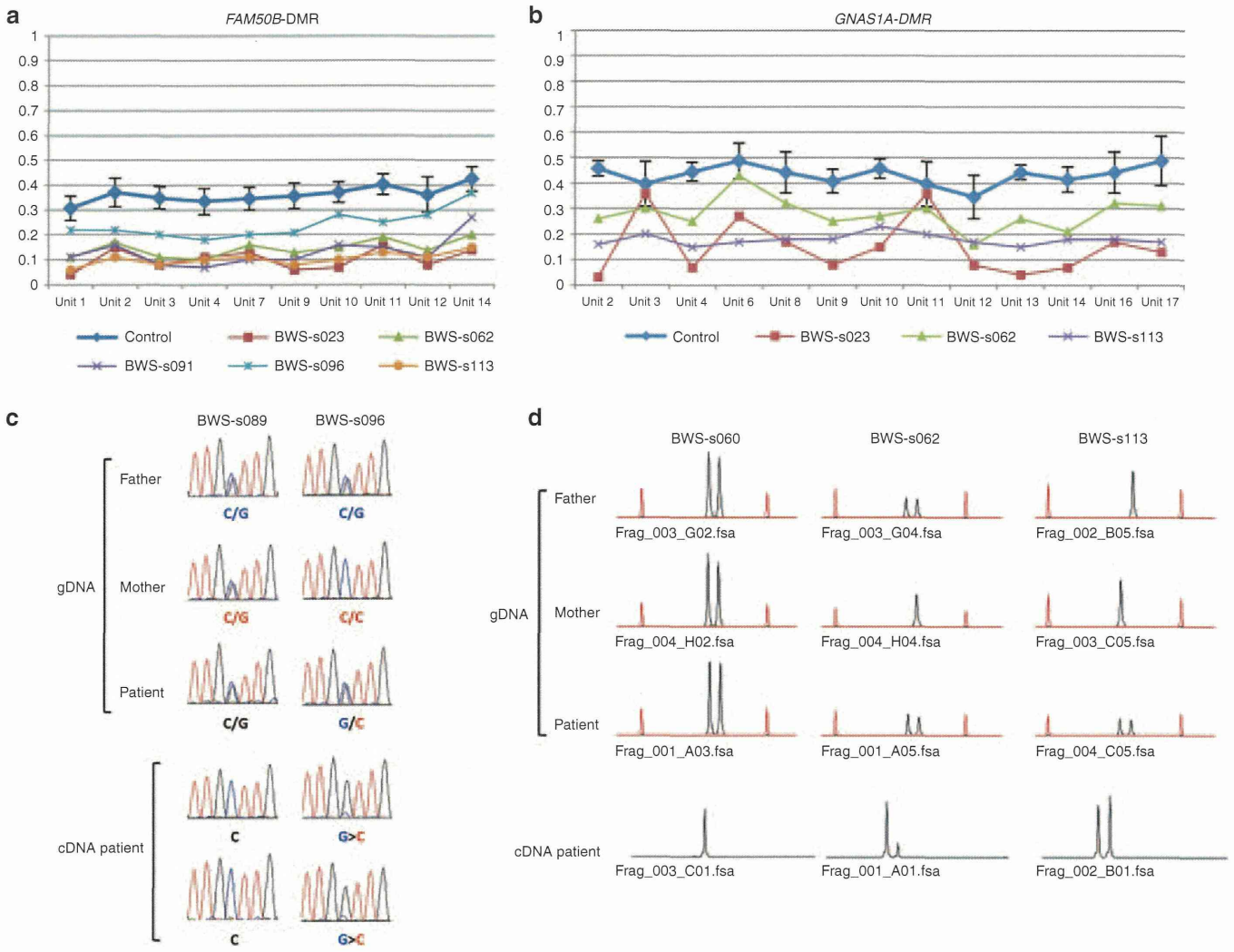

Figure 4 Methylation analysis of *FAM50B*- and *GNAS1A*-DMRs and expression analysis of the *FAM50B* and *GNAS1A* genes. (**a**,**b**) Results of matrix-assisted laser desorption/ionization mass spectrometry analysis. Averages with SD of 24 normal controls are shown in blue. Methylation indexes of patients showing LOM are indicated in different colors. Ten CpG units analyzed for *FAM50B*-DMR covered 13 CpG sites, and 13 CpG units analyzed for *GNAS1A*-DMR covered 18 CpG sites. (**c**) Results of expression analysis of the *FAM50B* gene. Beckwith–Wiedemann syndrome (BWS) patient BWS-s096 was heterozygous for a coding SNP (*rs6597007*) with LOM and showed biallelic expression with a low peak of maternal expression, whereas monoallelic expression was seen in a patient with normally methylated differentially methylated regions (DMRs) (patient BWS-s089). In patient BWS-s096, maternal expression was noted in two independent analyses despite low-grade LOM. gDNA, genomic DNA. (**d**) Results of expression analysis of the *GNAS1A* gene. Patients BWS-s062 and BWS-s113, heterozygous for a deletion/insertion variation (*rs143800311*) with LOM, showed biallelic expression, whereas patient BWS-s060 possessed normally methylated DMRs and exhibited monoallelic expression. Maternal expression was noted despite low-grade LOM in patient BWS-s062. Red peaks are molecular markers. GOM, gain of methylation; LOM, loss of methylation.

with X-chromosome inactivation and twinning.[29] This hypothesis suggests that females might tend to suffer from MMDs. We compared the frequency of female patients with MMDs with the frequency of those with monolocus methylation defects, but no significant difference could be found (Table 1).

DISCUSSION

Currently, most reports have studied 3–10 imprinted DMRs in BWS patients,[7–10,13] with the exception of two reports in which 16 and 27 DMRs were analyzed.[11,12] In addition, the quantitative capability of methods used for multiple methylation analyses has been variable, and few studies have conducted multiple checks to confirm the methylation statuses of all DMRs showing aberrant methylation.[7–13] To resolve these matters, we analyzed 29 DMRs and confirmed all aberrantly methylated DMRs using MALDI-TOF MS and bisulfite pyrosequencing, which are the most reliable quantitative methods of methylation analysis available at present.[19,30,31] We found that 34.1% of *Kv*DMR1-LOM patients exhibited MMDs. The frequency was higher than that in previous reports, which can be summarized as reporting an overall frequency of 20.6% (102 of 495 patients).[7–13] However, within these reports, the frequency in studies that analyzed 10 or fewer DMRs is 19.0% (82 of 431),[7–10,13] and the frequency in studies that analyzed more than 10 DMRs is 31.3% (20 of